

1           **The changing character of twenty-first century precipitation over the**  
2           **western United States in the variable-resolution CESM**

3           Xingying Huang, \* Paul A. Ullrich

4           *Department of Land, Air and Water Resources, University of California, Davis*

5           \*Corresponding author address: Xingying Huang, Department of Land, Air and Water Resources,  
6           University of California Davis, Davis, CA 95616.  
7           E-mail: xyhuang@ucdavis.edu

## ABSTRACT

8     The changing character of precipitation frequency and intensity in the west-  
9     ern United States over the 21st century is investigated using an ensem-  
10    ble of 26-year simulations with the variable-resolution Community Earth  
11    System Model (VR-CESM) at a local grid resolution of  $\sim 0.25^\circ$ . Simula-  
12    tions are forced using prescribed sea-surface temperatures, sea-ice extent and  
13    greenhouse gas concentrations from the representative concentration pathway  
14    (RCP) 8.5 scenario. VR-CESM is shown to be effective at accurately cap-  
15    turing the spatial patterns of the historical precipitation climatology. In the  
16    Intermountain West and Southwest U.S. we observe a statistically significant  
17    increase in mean precipitation and rainy days through mid-century, although  
18    this trend is tampered by end of century in response to a decrease in relative  
19    humidity. In the Pacific Northwest, extreme precipitation events are observed  
20    to increase significantly as a result of increased cool season integrated va-  
21    por transport. In particular, extreme precipitation in this region appears to  
22    increase more rapidly than would be predicted by the Clausius-Clapeyron re-  
23    lationship. No clear climate signal emerges in mean precipitation or for ex-  
24    tremes in California, where the precipitation climatology is subject to large  
25    interannual variability that is tied more closely to ENSO.

<sup>26</sup> **1. Introduction**

<sup>27</sup> There is substantial and growing interest in the character of precipitation within a changing  
<sup>28</sup> climate, largely due to pronounced impacts on water availability and flood management in both  
<sup>29</sup> human and natural systems (Hegerl et al. 2004; Kharin et al. 2007; Scoccimarro et al. 2013).  
<sup>30</sup> Among these studies, precipitation extremes have been a major focus, particularly drought and  
<sup>31</sup> flood events (Seneviratne et al. 2012). Overall, it is widely agreed that although atmospheric  
<sup>32</sup> water vapor concentration is increasing, the impacts of a changing climate on the character of  
<sup>33</sup> precipitation is far more complicated. Extreme precipitation events are particularly nuanced: Our  
<sup>34</sup> best projections suggest that extreme precipitation events will intensify even in regions where  
<sup>35</sup> mean precipitation decreases (Tebaldi et al. 2006; Kharin et al. 2007).

<sup>36</sup> Although future climate projections are subject to large uncertainties, climate models are essen-  
<sup>37</sup> tial tools for studying climate variability and extremes events in the future (Easterling et al. 2000).  
<sup>38</sup> Global climate models (GCMs) have often been used to investigate changes in the mean, vari-  
<sup>39</sup> ability and extremes of climate, as forced with predicted greenhouse gas (GHGs) concentrations  
<sup>40</sup> and aerosol emissions (Meehl et al. 2006). Several past studies have investigated global impacts  
<sup>41</sup> (Seneviratne et al. 2012), but studies addressing impacts at local and regional scales are less com-  
<sup>42</sup> mon. Although increased GHG concentrations have contributed to the observed intensification  
<sup>43</sup> of heavy precipitation events over the tropical ocean (Allan and Soden 2008) and the majority of  
<sup>44</sup> Northern Hemisphere overland areas (Min et al. 2011), these impacts are much more poorly un-  
<sup>45</sup> derstood at regional scales due to variability at finer spatial scales associated with the atmospheric  
<sup>46</sup> circulation (Trenberth 2011). As a consequence of this variability, confidence in the assessment of  
<sup>47</sup> regional extreme precipitation changes requires both high spatial resolution and a long integration  
<sup>48</sup> period, both of which can make the computational cost untenable for global simulations.

49 This issue of insufficient regional-scale climate information has been a major outstanding prob-  
50 lem in climate science, as stakeholders and water managers typically require fine-scale information  
51 on climate impacts in order to effectively develop adaptation and mitigation strategies. Dynamical  
52 downscaling with regional climate models (RCMs) has been one of the few tools available to  
53 ascertain the frequency, intensity, and duration of extreme events at the needed scales. By only  
54 simulating a limited regional domain, RCMs better capture fine-scale dynamical features with  
55 high horizontal resolution (Bell et al. 2004; Frei et al. 2006; Rauscher et al. 2010; Wehner 2013).  
56 Higher resolution enables more accurate simulation of precipitation extremes, which are driven by  
57 circulation patterns, cloudiness, land use, land/water contrast, snowpack and topography (Leung  
58 et al. 2003a; Diffenbaugh et al. 2005; Salathé Jr et al. 2008; Wehner et al. 2010). For example,  
59 Leung et al. (2003b) showed that the higher-resolution RCMs yield more realistic precipitation  
60 patterns and produce more frequent heavy precipitation over the western U.S. (WUS), consistent  
61 with observations. Diffenbaugh et al. (2005) studied both extreme temperature and precipitation  
62 events over the contiguous United States using a RCM configured at 25 km horizontal resolu-  
63 tion, and demonstrated that fine-scale processes were critical for accurate assessment of local- and  
64 regional-scale climate change vulnerability. Salathé Jr et al. (2008) found significant differences in  
65 trends for temperature and precipitation over the Pacific Northwest using a high-resolution RCM  
66 for future climate simulations. And Ashfaq et al. (2016) observed a 7.4% increase in precipitation  
67 from extremes over the contiguous U.S. from simulations with RegCM4 driven by CMIP5 global  
68 data.

69 Despite their success, RCMs also have known issues associated with inconsistency between  
70 the lateral forcing data and the driven RCM. The menu of physical parameterizations and tuning  
71 parameters typically available to RCMs can also lead to over-tuning of the model for a partic-  
72 ular geographic region or climatological field (McDonald 2003; Laprise et al. 2008; Mesinger

and Veljovic 2013). Consequently, there has been growing interest in variable-resolution enabled GCMs (VRGCMs) to improve regional climate simulations. Unlike RCMs, which require GCM data to drive the simulation at lateral boundaries, VRGCMs use a unified model with coarse global resolution and enhanced resolution over a specific study region (Staniforth and Mitchell 1978; Fox-Rabinovitz et al. 1997). VRGCMs have demonstrated competitive ability for regional climate studies at a reduced computational cost, particular when compared to uniform-resolution GCMs (Fox-Rabinovitz et al. 2006; Rauscher et al. 2013).

In this paper, we utilize the recently developed variable-resolution option in the Community Earth System Model (VR-CESM). VR-CESM is based on the CESM (and its predecessor, the Community Climate System Model (CCSM)), a family of models that have been used for decades to study the global climate (Neale et al. 2010a; Hurrell et al. 2013). The overall performance of VR-CESM for modeling regional climate in the California and Nevada is detailed in Huang et al. (2016), where it was argued that VR-CESM has competitive biases in comparison to the Weather Research and Forecasting (WRF) model (a traditional RCM) and the uniform-resolution CESM, when evaluating against high-quality observations and reanalysis. VR-CESM has been used in a number of studies to simulate fine-scale atmospheric processes (Zarzycki et al. 2014, 2015; Rhoades et al. 2015; Huang and Ullrich 2016; Rhoades and Zarzycki 2016).

This study focuses on changes in the character of precipitation over the 21st century within the WUS, as predicted from long-term ensemble runs conducted with VR-CESM with a local grid resolution of  $\sim 0.25^\circ$ . The WUS is known to be particularly vulnerable to hydrological extremes, particularly floods and droughts (Leung et al. 2003b; Caldwell 2010), and hosts a variety of local features and microclimates associated with its rough and varied topography. Simulations of the future climate are performed in accordance with the representative concentration pathway (RCP) 8.5 scenario, which describes a “business-as-usual” projection for GHGs (Riahi et al. 2011). In this

study we focus singularly on the RCP 8.5 scenario because its mid-century results are similar to a more optimistic RCP2.6 scenario end-of-century. Simulations are further conducted in accordance with the Atmospheric Model Intercomparison Project (AMIP) protocol (Gates 1992), a widely-used approach for climate model diagnosis, validation and intercomparison that imposes global sea surface temperatures (SSTs) and sea ice. It is well-known that correctly simulating changes to the spatial pattern of SSTs in state-of-the-art coupled GCMs remains a significant challenge (Joseph and Nigam 2006; Stevenson 2012; Jha et al. 2014; Taschetto et al. 2014). However, by constraining atmospheric boundary conditions at the sea surface, we avoid model biases that are known to exist in the fully coupled configuration (Grodsy et al. 2012; Small et al. 2014) and accept potential uncertainties associated with our choice of SSTs.

Changes in the character of precipitation, in terms of frequency and intensity, have been assessed in our study from recent history through the end of the 21st century. A comprehensive set of metrics for precipitation extremes have been evaluated from the ensemble simulations over the 26-year periods corresponding to historical (1980-2005), mid-century (2025-2050) and end-of-century (2075-2100). We hypothesize that spatial inhomogeneity in local geography and temperature will also result in similarly inhomogeneous impacts on the precipitation field. We further expect that teleconnections (specifically the El Niño-Southern Oscillation, ENSO) will have a pronounced impact on precipitation features. Since only one SST dataset was used for this study, we note that our projections are conditioned on a particular future character of ENSO. This is a potentially large source of uncertainty, as at present there is no clear consensus on how ENSO may behave under a warming climate (Fedorov and Philander 2000; Latif and Keenlyside 2009; Guilyardi et al. 2009; Collins et al. 2010; DiNezio et al. 2012), and strengthening or weakening of this pattern will have clear consequences for our results (as discussed in section 6d).

120 This work builds on a number of previous studies that have explored the projected future change  
121 in WUS precipitation. For example, Kim (2005) applied downscaled climate change signals to se-  
122 lected indicators, and concluded that global warming induced by increased CO<sub>2</sub> is likely to drive  
123 increases in extreme hydrologic events in the WUS. Duffy et al. (2006) found that changes to  
124 mean precipitation predicted by the RCMs are not statistically significant compared to interannual  
125 variability in many regions over WUS, although there is little consistency among the different  
126 RCMs as to responses in precipitation to increased GHGs. Gao et al. (2015) pointed out a poten-  
127 tially large increase in atmospheric river events by the end of the 21st century under the RCP8.5  
128 scenario, with implications for large-scale and heavy precipitation events along the Pacific coast.

129 This paper is structured as follows. Section 2 describes the model setup. Section 3 describes  
130 the methodology and reference datasets employed. An assessment of the ability of the model to  
131 capture the climatology of the WUS is given in section 4. Results from the future mean climato-  
132 logical trend and projected changes to precipitation indices are in section 6. Section 7 summarizes  
133 the main points of the study along with further discussion.

## 134 2. Model Setup

135 CESM is a state-of-the-art Earth modeling framework, consisting of coupled atmosphere, ocean,  
136 land and sea ice models (Neale et al. 2010b; Hurrell et al. 2013). In this study, the Community At-  
137 mosphere Model version 5 (CAM5) (Neale et al. 2010b) and the Community Land Model version  
138 4.0 (Oleson et al. 2010) are used. CAM5 is configured with the Spectral Element (SE) dynamical  
139 core, which is known for its conservation properties, accuracy and parallel scalability (Dennis et al.  
140 2011; Taylor 2011) and incorporates the variable-resolution option (Zarzycki et al. 2014). CLM  
141 is employed in the *unigrid* configuration, which allows the land model and atmospheric model to  
142 utilize the same model grid so eliminates the need for interpolation. SSTs and sea ice, which are

<sup>143</sup> used to compute ocean-atmosphere fluxes, are prescribed in accordance with the AMIP protocol  
<sup>144</sup> (Gates 1992). The variable-resolution mesh used for this study is depicted in Figure 1, in accord  
<sup>145</sup> with our past studies (Rhoades et al. 2015; Huang et al. 2016; Huang and Ullrich 2016; Rhoades  
<sup>146</sup> and Zarzycki 2016).

<sup>147</sup> Simulations have been performed for the historical period (1979-2005, hereafter referred to as  
<sup>148</sup> hist) and for two future periods: 2024-2050 (hereafter referred to as mid) and 2074-2100 (hereafter  
<sup>149</sup> referred to as end). Daily output are recorded for each period on the native SE grid and then  
<sup>150</sup> remapped to a regional latitude-longitude mesh (Ullrich and Taylor 2015; Ullrich et al. 2016). For  
<sup>151</sup> purposes of analysis, the first year of each time period was discarded as a spin-up period to allow  
<sup>152</sup> adequate time for the initialized land and atmosphere to equilibrate. The 26-year duration was  
<sup>153</sup> chosen to provide an adequate sampling of annual variability for each time phase. As mentioned  
<sup>154</sup> earlier, GHG concentrations are set based on RCP8.5. Historical SSTs and sea ice are prescribed  
<sup>155</sup> at  $1^{\circ}$  resolution, as described by Hurrell et al. (2008). SSTs and sea ice for each future period are  
<sup>156</sup> developed from fully-coupled RCP 8.5 climate simulations with bias correction applied (Cecile  
<sup>157</sup> Hannay, personal communication). Annually-updated land surface datasets, which prescribe land-  
<sup>158</sup> use characteristics, are interpolated from  $0.5^{\circ}$  to the land model grid.

<sup>159</sup> Ensemble runs are needed to ensure that the sample adequately accounts for climate variability,  
<sup>160</sup> especially for statistics associated with climatological extremes. However, the exact number of  
<sup>161</sup> ensemble members required is heavily dependent on the variability of the particular metric being  
<sup>162</sup> examined, and so no standard ensemble criteria exists. Deser et al. (2012b) suggest that around  
<sup>163</sup> 3 ensemble runs are required to detect a significant epoch difference for JJA (June-July-August)  
<sup>164</sup> surface temperatures, whereas 10 to 30 ensemble members are needed for that for DJF (Dec.-Jan.-  
<sup>165</sup> Feb.) precipitation. In our study, the use of prescribed SSTs does reduce the intrinsic variability

<sup>166</sup> of the climate system (see supplement), and so we found reasonably converged results with two  
<sup>167</sup> ensemble members for the historical period and four ensemble members for each future period.

<sup>168</sup> **3. Methodology**

<sup>169</sup> *a. Precipitation indices*

<sup>170</sup> Standard indices have been employed to characterize precipitation (Tebaldi et al. 2006; Zhang  
<sup>171</sup> et al. 2011; Sillmann et al. 2013). In order to choose a comprehensive (but minimal) set that are  
<sup>172</sup> informative to stakeholders and water managers, indices from throughout the literature have been  
<sup>173</sup> assessed. The indices examined include those defined by the Expert Team on Climate Change  
<sup>174</sup> Detection and Indices (ETCCDI) (Karl et al. 1999) that are featured in earlier studies (Dulière  
<sup>175</sup> et al. 2011; Sillmann et al. 2013; Diffenbaugh et al. 2005; Singh et al. 2013) and others such as  
<sup>176</sup> return levels, dry spell and wet spell characteristics defined by either percentiles or by selected  
<sup>177</sup> thresholds. As a result, the indices we have chosen for this study attempt to provide a relatively  
<sup>178</sup> comprehensive characterization of precipitation, and are summarized in Table 1. Indices related to  
<sup>179</sup> dry spells of variable duration have been investigated in this study, but only exhibited meaningful  
<sup>180</sup> differences for dry spell periods under 5 days and so are not discussed.

<sup>181</sup> *b. Impacts of ENSO*

<sup>182</sup> The impact of ENSO on precipitation is emphasized in our study due to its influence on precipi-  
<sup>183</sup> tation over a majority of our study area, particularly the southwest U.S. (Cayan et al. 1999; Zhang  
<sup>184</sup> et al. 2010; Deser et al. 2012a; Yoon et al. 2015). The phase of ENSO (*i.e.* El Niño and La Niña)  
<sup>185</sup> is identified each year using the Oceanic Niño Index (ONI), defined as the 3-month running means  
<sup>186</sup> of SST anomalies in the Niño 3.4 region (covering 5N-5S, 120-170W based on NOAA (2013)).  
<sup>187</sup> An El Niño or La Niña episode is said to occur when the ONI exceeds +0.5 or -0.5 for at least five

188 consecutive months for a water year (i.e. from July to June) (NOAA 2013) (see the supplement).

189 In order to adjust for the trend in the SST field associated with climate change, the anomaly is  
190 computed against the detrended mean SSTs from the periods 1971-2000, 2020-2050 and 2070-  
191 2100 for `hist`, `mid` and `end` respectively, using the aforementioned observed and predicted SST  
192 datasets. As argued by Kao and Yu (2009), it may be desirable to use an extended Niño 3.4 region  
193 to determine the phase of ENSO – however, when employing SST anomalies integrated over the  
194 region 105-170W, we observed no significant impact on ONI statistics.

195 *c. Assessing statistical significance*

196 Student's t-test has been used to determine whether or not two datasets at each grid point are  
197 statistically equivalent, if the sample population can be adequately described by a normal distri-  
198 bution. The normality of a dataset is assessed under the Anderson-Darling test. When the sample  
199 populations do not approximately follow a normal distribution, Mann-Whitney-Wilcoxon (MWW)  
200 test is employed in lieu of the t-test. All these tests are evaluated at the 0.05 ( $\alpha$ ) significance level.  
201 When comparing different time periods, statistical tests are conducted by treating all years from  
202 all ensemble members as independent samples ( $26 \times 2$  sample years for `hist` and  $26 \times 4$  sample  
203 years for `mid` and `end`).

204 (add description of the supplement like what are included; see the `sst_enso.pdf`, mask the land  
205 (over land, it should be the surface temperature.))

206 *d. Reference datasets*

207 Gridded observational datasets and reanalysis of the highest available quality, with comparable  
208 horizontal resolutions to our VR-CESM simulations, are used for assessing the simulation qual-

209      ity. Multiple reference datasets are necessary due to the underlying uncertainty in interpolating  
210      precipitation fields. The three datasets employed are as follows:

211      **UW Gridded Data:** The  $0.125^{\circ}$  UW daily gridded meteorological data is obtained from  
212      the Surface Water Modeling group at the University of Washington, covering the period  
213      1949-2010 (Maurer et al. 2002; Hamlet and Lettenmaier 2005). The UW dataset imposes  
214      topographic corrections by forcing the long-term average precipitation to match that of the  
215      Parameter-elevation Regressions on Independent Slopes Model (PRISM) dataset.

216      **National Centers for Environmental Prediction (NCEP) Climate Prediction Center**  
217      **(CPC):** The  $0.25^{\circ}$  CPC daily dataset provides gauge-based analysis of daily precipitation cov-  
218      ering the period 1948-2006. It is a unified precipitation product that covers the Conterminous  
219      United States and amalgamates a number of data sources at CPC via optimal interpolation  
220      objective analysis.

221      **North American Regional Reanalysis (NARR):** NARR is a  $\sim 32$  km high-resolution reanal-  
222      ysis product with 3-hourly output produced by NCEP via dynamical downscaling over North  
223      America and covering the period 1979-present (Mesinger et al. 2006).

#### 224      **4. Assessment of Precipitation Character in VR-CESM**

225      Before proceeding, we assess the ability of VR-CESM to represent the character of precipitation  
226      over the WUS. The indices defined in Table 1 are depicted in Figures 2, 3 and 4 for VR-CESM  
227      and each of the reference datasets over the historical period (1980-2005). We assume equal con-  
228      fidence in each of the reference datasets, and use Student's t-test (with UW, CPC and NARR as  
229      the three statistical samples) to identify regions where VR-CESM deviates significantly from the

230 reference mean. Regions where differences are statistically significant in the VR-CESM dataset  
231 are identified with stippling.

232 Overall, VR-CESM largely captures the spatial patterns of precipitation and its indices. As ex-  
233 pected, the majority of precipitation is distributed along the northwest coastal area and the moun-  
234 tainous regions of the Cascades and the Sierra Nevada. Nonetheless, several apparent biases are  
235 present:

236 First, VR-CESM significantly overestimates Pr over dry regions with differences between 0.2  
237 mm to 1.5 mm, and over the eastern flank of the Cascades and on both sides of the Sierra Nevada  
238 (with relative differences reaching 50%-150%). As with many regional models, VR-CESM is  
239 “dreary” and exhibits too many precipitation days ( $R_{1mm}$ ,  $Pr \geq 1$  mm/day and  $R_{5mm}$ , 1 mm/day  $\leq$   
240  $Pr \leq 5$  mm/day) (see Figure 3) (Stephens et al. 2010). Nonetheless, over most regions the relative  
241 contribution of each precipitation frequency subset to total precipitation ( $F_{1mm}$ ,  $F_{5mm}$ ,  $F_{10mm}$ ,  
242  $F_{20mm}$  and  $F_{40mm}$ ) agrees well, suggesting that the frequency distribution describing precipita-  
243 tion intensity is accurately simulated almost everywhere.

244 Second, the spatial pattern of precipitation intensity (SDII) agrees well between VR-CESM  
245 and references with agreement everywhere except in the Great Plains (the eastern edge of our  
246 domain) and in California’s Central Valley. The Great Plains is not a focus of this study, but  
247 the suppressed intensity is primarily during the warm season (April-September) and so likely  
248 represents a failure of the convection scheme to adequately simulate variability in this region.  
249 This bias is also observed in  $0.25^\circ$  uniform-resolution CESM simulations (Small et al. 2014), and  
250 so is not a symptom of the eastern edge of the variable-resolution transition region.

251 However, the grossly exaggerated intensity over the western flank of the Sierra Nevada through  
252 California’s Central Valley does merit some additional discussion. Here, the overestimation of pre-  
253 cipitation and enhanced intensity is associated with too many extreme precipitation events ( $Pr > 20$

254 mm/day) (see Figure 4, F40mm and Fxmm). This bias is related to exaggerated orographic uplift  
255 (upslope winds, not shown) and triggers a dry bias along the eastern flank of the Sierras. Similar  
256 biases in simulating extreme precipitation over topographically complex regions have also been  
257 found in high-resolution RCM simulations, and have been primarily attributed to excessively strong  
258 winds (Walker and Diffenbaugh 2009; Singh et al. 2013). This issue may be further impacted by  
259 the diagnostic treatment of precipitation in CAM5 (Morrison and Gettelman 2008; Gettelman et al.  
260 2008).

261 The representation of precipitation in VR-CESM over California was also discussed in Huang  
262 et al. (2016), where it was observed that VR-CESM simulations at  $0.25^{\circ}$  adequately represented  
263 regional climatological patterns with high spatial correlation. VR-CESM demonstrated compa-  
264 rable performance to WRF at 27 km (which was forced with ERA-Interim reanalysis), but still  
265 overestimated overall winter precipitation compared to reference datasets (by about 25%-35%),  
266 with the largest differences over the western edge of the Sierra Nevada. This bias is not allevi-  
267 ated by simply increasing the spatial resolution, as experimental VR-CESM simulations at 14km,  
268 7km and 3.5km show only modest improvement (Alan M. Rhoades, personal communication).  
269 This suggests that the bias might be related with more complex dynamic processes rather than  
270 treatment of the orographic effects.

271 CESM at  $1^{\circ}$  resolution was also assessed in order to better understand the impacts of resolu-  
272 tion. We find that precipitation patterns over complex topography are poorly represented in the  $1^{\circ}$   
273 dataset and do not capture the spatial patterns induced by orographic effects. Over the Cascades  
274 and Sierra Nevada, total precipitation is grossly underestimated by  $1^{\circ}$  CESM, when compared to  
275 VR-CESM, gridded and reanalysis datasets (see the supplement [[Point to exact figure](#)]). Precip-  
276 itation has otherwise been smoothed out over the coastal areas and the mountainous regions of  
277 the northwest U.S when simulated with CESM at coarse resolution. This result clearly under-

278 scores the benefits of high resolution (particularly the representation of topography) in simulating  
279 precipitation features. Results are also provided in the supplement for the output from a globally-  
280 uniform CESM run at  $0.25^{\circ}$  spatial resolution with the finite volume (FV) dynamical core (Wehner  
281 et al. 2014), which exhibits similar performance to VR-CESM (see the supplement [Point to exact  
282 figure]). Overall,  $0.25^{\circ}$  resolution appears to provide the best tradeoff between accuracy and com-  
283 putational cost, as coarser resolution does not correctly represent precipitation features and higher  
284 resolution does not appear to substantially improve model accuracy.

285 We have also assessed the impact of the ENSO signal within the historical VR-CESM runs by  
286 differencing the precipitation fields between the warm phase (i.e. El Niño) and cool phase (i.e.  
287 La Niña), compared to references (see the supplement). ENSO exhibits a weaker signal for obser-  
288 vational precipitation, compared to VR-CESM, which might suggest that the model exaggerates  
289 ENSO's impact on precipitation, especially over the northwest U.S. The improvement of ENSO  
290 in the model is directly proportional to the representation of ENSO-forced precipitation anomalies  
291 (AchutaRao and Sperber 2006).

## 292 **5. Drivers of Climatological Precipitation Change**

293 The remainder of this paper now focuses on model predictions of change over the 21st cen-  
294 tury. Precipitation has been observed and modeled to be modified in character at both global and  
295 regional scales under climate change. The observed intensification of heavy precipitation events  
296 over the recent past for the majority of Northern Hemisphere land areas is primarily attributed  
297 to increases in GHGs (Min et al. 2011). GHGs drive radiative changes in the lower troposphere,  
298 increase SSTs and lead to increased evaporation, all of which then impact the character of precip-  
299 itation events (Allen and Ingram 2002; Sugi and Yoshimura 2004). Several studies have argued  
300 that precipitation extremes will intensify continuously through the end of 21st century in both dry

301 and wet regions, although the extent of this change will be spatially heterogeneous (Donat et al.  
302 2016).

303 In accordance with the Clausius-Clapeyron (C-C) relationship, saturation vapor pressure in the  
304 atmosphere is expected to increase by  $\sim 7\%$  for each  $1^{\circ}\text{C}$  increase in temperature (Allan and So-  
305 den 2008). As long as a source of water vapor is present, a corresponding increase in atmospheric  
306 water vapor content is expected. Naturally, evaporation over the ocean will increase with climate  
307 warming, but increases in water vapor content over land may be constrained by soil moisture  
308 (Cayan et al. 2010). When specific humidity is high, heavy rain events become more probable,  
309 even if total precipitation is decreasing (Trenberth 2011). This suggests that global total precipi-  
310 tation is expected to increase at a slower rate than precipitation extremes (Allan and Soden 2008).

311 In accordance with previous studies (e.g. (Allan and Soden 2008; O’Gorman and Schneider 2009;  
312 Min et al. 2011)), changes to extreme precipitation follow the C-C relationship more closely than  
313 total precipitation amount (Trenberth et al. 2003). However, there is still substantial uncertainty  
314 for the magnitude of the change, since precipitation extremes are also dependent on factors such  
315 as the vertical velocity profile and temperature (O’Gorman and Schneider 2009).

316 With overland water vapor constrained by soil moisture content, changes to moderate or heavy  
317 precipitation events over the WUS are mainly the result of increased large-scale vapor transport  
318 from the eastern Pacific Ocean rather than directly from evaporation, typically associated with  
319 atmospheric rivers (ARs) and/or orographic uplift (Trenberth et al. 2003; Neiman et al. 2008).

320 Warming may lead to enhancement of the storm track, which would increase ARs along the U.S.  
321 west coast with increased air water vapor content in the future (Dettinger 2011; Gao et al. 2015).

322 In the following sections, both the mean changes of precipitation and distributions of both non-  
323 extreme and extreme events are investigated as projected by the VR-CESM model under climate  
324 forcing.

325 The precipitation of the WUS has strong inter-annual variability caused by large-scale atmo-  
326 spheric circulation mainly associated with the ENSO (Leung et al. 2003b). As a significant  
327 driver of precipitation, ENSO modulates the storm track behavior over western U.S. with a north-  
328 west/southwest precipitation dipole (Gershunov and Barnett 1998), as discussed in d. The pro-  
329 jected SSTs used in this study emerge from one possible outcome for ENSO. However, there is  
330 still substantial uncertainty regarding how El Niño will change under global warming (Fedorov  
331 and Philander 2000; Guilyardi et al. 2009), which is a source of uncertainty in our results. Capo-  
332 tondi (2013) showed that the diversity of El Niño characteristics in CCSM4 is comparable to what  
333 was found in observations, although, as found by Deser et al. (2012c), the overall magnitude of  
334 ENSO in CCSM4 [Paul: was this changed at all in CESM1?] is overestimated by 30% over the  
335 preindustrial time period.

## 336 6. Results

### 337 a. Mean climatology

338 The mean climatological changes in VR-CESM across time periods are depicted in Figure 5.  
339 Since the character of WUS precipitation has a strong seasonal contrast, changes to mean precipi-  
340 tation, near-surface temperature and near-surface relative humidity are depicted for what we refer  
341 to as the cool season (October to March) and the warm season (April to September).

342 As a result of enhanced GHG concentrations, mean annual near-surface temperature ( $T_{avg}$ )  
343 increases by about 1.5 to 2 K from hist to mid and about 4 to 6 K from mid to end. Despite the  
344 large spatial variation in mean seasonal temperatures, the observed change to mean temperature is  
345 fairly uniform, particularly over the ocean and in coastal regions. Away from the coast there is a  
346 weak gradient in the temperature change field, with the largest increase in temperatures occurring

347 towards the northeast during the cool season and towards the north during the warm season. The  
348 increase in temperature is also about 0.5K and 1.0K larger during the warm season compared to  
349 the cool season for mid and end, respectively.

350 Overall, future RH is constrained closely to hist since it is governed by competing increases in  
351 temperature and atmospheric water vapor content. Although RH increases monotonically over the  
352 ocean in response to increased evaporation, over land the character is more heterogeneous: In gen-  
353 eral, RH tends to increase in regions where Tavg increase is constrained below  $\sim$  2 K, but decrease  
354 when Tavg anomaly exceeds  $\sim$  2 K. The decrease in these regions is on the order of 2% and 3-6%,  
355 compared to mid and end respectively. In fact, trends in RH are spatially consistent with tempera-  
356 ture increase but opposite in magnitude with a spatial correlation coefficient of approximately 0.8.  
357 This suggests that continental evaporation and oceanic water vapor transport are insufficient vapor  
358 sources when temperature reaches a certain level, consistent with the observation of Joshi et al.  
359 (2008). This effect has also been observed in results by Rowell and Jones (2006) over continental  
360 and southeastern Europe and Simmons et al. (2010) over low-latitude and midlatitude land areas.

361 In response to these changes to temperature and RH, from hist to mid mean precipitation over  
362 the entire domain exhibited a 0.2-0.6 mm/day increase during the cool season. The largest changes  
363 were over northwest, where cool-season precipitation emerges from large-scale patterns (namely,  
364 atmospheric rivers and associated storm systems)(Trenberth et al. 2003; Neiman et al. 2008). Over  
365 the warm season, where precipitation in the WUS is primarily from convection, the increase was  
366 around 0.2 mm/day through the intermountain west and southwest with drying through the north-  
367 west (a decrease in mean precipitation of 0.2 mm/day). These trends largely hold and intensify  
368 through end, except in the intermountain west and southwest regions where precipitation again  
369 falls to historical levels. Statistical significance of these results is depicted in Figure 6.

370 The increase in cool season precipitation in the Northwest is largely driven by increased inte-  
371 grated vapor transport (IVT) (see Figure 8a,b) during extreme precipitation events. IVT is par-  
372 ticularly useful for understanding extreme precipitation events that arise from large-scale meteo-  
373 rological features (Ralph et al. 2004; Leung and Qian 2009; Dettinger 2011). IVT is composed  
374 of absolute humidity and wind velocity, which are both impacted by the climate change signal.  
375 To understand how these two factors respond to the climate change signal and contribute to the  
376 increase in IVT, specific humidity and wind vectors are plotted in Figure 8b. Over the eastern  
377 Pacific, we observe increases in both water vapor content and wind speed, which are in turn re-  
378 sponsible for increases to IVT in the Pacific Northwest. However, over the continent we see a  
379 weakening of the westerlies overland driven by a reduced meridional temperature contrast. The  
380 increased cool-season IVT does not manifest strongly along the Pacific coast off of California,  
381 where IVT is much smaller on average and is primarily modulated by ENSO.

382 Changes in precipitation over the Intermountain West and Southwest during the warm season are  
383 primarily associated with convective processes and so are directly impacted by variations in RH.  
384 As shown in Figure 5, RH increases through mid-century in this region (although with modest  
385 significance) and then significantly decreases through end-of-century over most the study area  
386 (except over where soil moisture was already low in hist). This results in a modest increase in  
387 precipitation through mid-century followed by a return to historical precipitation amounts by end-  
388 of-century. Further climate warming is expected to further decrease RH and drive increased aridity  
389 in this region.

390 *b. Precipitation indices*

391 We now analyze observed changes to the precipitation indices given in Table 1. For each index,  
392 the change for each period, yearly averaged over all ensemble members are plotted in Figure 6 (for

393 the indices that quantify precipitation days) and Figure 7 (for the indices describing precipitation  
394 amounts).

395 On comparing `hist` and `mid`, it is clear that the number of rainy days and frequency of non-  
396 extreme precipitation events ( $\leq 10$  mm/day) have increased significantly (about 10-15%) over the  
397 southwest and intermountain west, which is less obvious between `mid` and `end`. On the contrary,  
398 the frequency of non-extreme precipitation have decreased significantly over the northwest region  
399 and the eastern areas of the Montana, Wyoming and Oregon (by about 10%). The increase in  
400 the frequency of these non-extreme precipitation events explain the observed change to mean  
401 precipitation exhibited in Figure 5, and are largely associated with warm season mesoscale storm  
402 systems.

403 Although essentially all regions exhibit an increase in the extreme precipitation events ( $Pr \geq 10$   
404 mm/day), this increase is only statistically significant through the intermountain west and in the  
405 Pacific northwest (for  $Pr \geq 20$  mm/day). When comparing `mid` to `end`, there is a clear and sig-  
406 nificant increase in extreme precipitation events over the northwest coast (~ 20-30%) and eastern  
407 flank of the Cascades ( $> 40\%$ ). This result is consistent with the result of Dominguez et al. (2012),  
408 who observe a robust increase in winter precipitation extremes toward the latter half of the 21st  
409 century with an ensemble of RCMs. The increase in the northwest is accompanied by a decrease  
410 in non-extreme precipitation days, indicative of drying over the warm season.

411 Notably, our results show no significant changes in mean precipitation or precipitation extremes  
412 are predicted for California. In fact, the precipitation signal under a warmer climate is more  
413 ambiguous for California (Neelin et al. 2013) in light of the extreme variability of the region on  
414 interannual time scales (Dettinger 2011). Kim (2005) found that under global warming, heavy  
415 precipitation events increase in frequency in the mountainous regions of the northern California  
416 Coastal Range and the Sierra Nevada. However, our results show a small decrease in extreme

<sup>417</sup> precipitation over the Sierra Nevada (although the decrease is not statistically significant). This  
<sup>418</sup> leads us to the likely conclusion (particularly in light of VR-CESM's own biases in this region)  
<sup>419</sup> that projections in this region are highly dependent on model formulation.

<sup>420</sup> For the most extreme precipitation events ( $\text{Pr} \geq 40 \text{ mm/day}$ ), there is a statistically significant  
<sup>421</sup> increase along the northwest coast ( $\geq 60\%$ ), the Cascades ( $\sim 50\%$ ) and Northern Rockies ( $\geq 60\%$ )  
<sup>422</sup> by end-of-century. Significant increases are also apparent along the Klamath range in California  
<sup>423</sup> of about 20-40% from hist to end. Changes in accumulated precipitation for these events are con-  
<sup>424</sup> sistent with the change in their frequency (see Figure 7). With a projected increase of temperatures  
<sup>425</sup> in this region of 4-5 K over the cool season, this increase is in excess of the 7% per degree change  
<sup>426</sup> that would be anticipated from the C-C relationship (Figure 8a). In this case, the probable cause  
<sup>427</sup> of this excess is due to the intensification of the storm track along the coast discussed in section a.

#### <sup>428</sup> c. *Regional precipitation frequency distributions*

<sup>429</sup> To further investigate the regional heterogeneity of changing precipitation, frequency distribu-  
<sup>430</sup> tions of daily rainfall for rainy days are plotted in Figure 9 for (a) the Pacific Northwest, including  
<sup>431</sup> Washington and Oregon, (b) California, (c) the Intermountain West, including Nevada and Utah  
<sup>432</sup> and (d) the Southwest, including Arizona and New Mexico. Frequency plots are developed using  
<sup>433</sup> simulation outputs at all grid points within each region. Over the Northwest, precipitation intensi-  
<sup>434</sup> fies with upper tail going more extreme in the future, especially during end. No apparent changes  
<sup>435</sup> can be observed for the California region, except with more extreme upper tail for Pr exceeding  
<sup>436</sup> 100 mm/day during end, which is due to the increased precipitation extremes over the northern  
<sup>437</sup> California as shown in Figure 7. Over the inter-mountainous region, similar trends of changes can  
<sup>438</sup> be seen as the northwest area, with intensified mean and extreme precipitation. For the southwest

<sup>439</sup> area, precipitation tends to be more extreme with a moderate level, although no notable difference  
<sup>440</sup> exists between mid and end.

<sup>441</sup> *d. Disentangling the direct climate signal from ENSO and PDO*

<sup>442</sup> As discussed earlier, this study assumes a fixed pattern of SSTs that is consistent across all  
<sup>443</sup> ensemble members and incorporates certain assumptions on the character of ENSO through the  
<sup>444</sup> end-of-century that arise from the coupled model. The phase of ENSO is well known to have  
<sup>445</sup> important repercussions for precipitation extremes (Larkin and Harrison 2005; Allan and Soden  
<sup>446</sup> 2008; Maloney et al. 2014; Yoon et al. 2015). In particular, Cai et al. (2014) found a significant  
<sup>447</sup> increase in extraordinary precipitation events through the eastern Pacific Ocean in the 21st century  
<sup>448</sup> within the CMIP5 ensemble, associated with increasing frequency of extreme El Niño events due  
<sup>449</sup> to greenhouse warming. To better understand how ENSO has impacted our results, we now turn  
<sup>450</sup> our attention to understanding how precipitation extremes behave in response to the phase of  
<sup>451</sup> ENSO.

<sup>452</sup> In our study, mean SSTs over the Niño 3.4 region are 26.83, 28.62 and 30.54°C for hist, mid and  
<sup>453</sup> end respectively. Based on the ONI index values, the mean SST anomalies over Niño 3.4 region  
<sup>454</sup> are 1.38, 1.71 and 2.30 K during El Niño years, and -1.16, -1.62 and -1.43 K during La Niña years,  
<sup>455</sup> again for hist, mid and end. It is apparent within that within this dataset the magnitude of SST  
<sup>456</sup> anomalies associated with ENSO has intensified. SST anomalies of each year and each month,  
<sup>457</sup> and their associated spatial pattern when averaged over the warm and cool phases of ENSO can  
<sup>458</sup> be found in the supplement, suggesting an increasing frequency of El Niño through mid and an  
<sup>459</sup> almost doubled frequency of La Niña during mid and end compared to the hist.

<sup>460</sup> [Huang: As SSTs increase in the future, is not it normal for the anomaly of ENSO to be increased  
<sup>461</sup> to compensate the changes of water vapor capacity? Might email Neale about this]

462 Differences in mean precipitation and associated indices taken between the warm phase (i.e.  
463 El Niño) and cool phase (i.e. La Niña) of ENSO are provided in Figure 10 for the cool seasons  
464 from hist, mid and end. During the El Niño phase, intensified mean precipitation is expected  
465 over California and the southwest (Hamlet and Lettenmaier 2007), accompanied by reduced pre-  
466 cipitation intensity over the northwest. In the La Niña phase, this pattern is reversed, with wetter  
467 conditions in the northwest and a drier southwest. Consequently, ENSO is associated with a  
468 northwest/southwest precipitation dipole, triggered by ENSO's modification of the storm track  
469 (Gershunov and Barnett 1998; Leung et al. 2003b), along with modulation of the enhanced pre-  
470 cipitation variability (Cayan et al. 1999; Kahya and Dracup 1994). Strengthening storm patterns  
471 associated with ENSO are also found by Maloney et al. (2014) over California using CMIP5  
472 output under RCP8.5. This dipole is also apparent in the frequency of rainy days and extreme  
473 precipitation events.

474 The impact of ENSO can also be seen in the IVT difference that arises between El Niño and  
475 La Niña phases in each time period (see Figure 11) and the accompanying 850 hPa wind patterns.  
476 During the El Niño phase, there is an increase in on-shore moisture flux over California that  
477 triggers a returning circulation through the northwest. This suggests that understanding moisture  
478 flux regulation from ENSO is a very important contributor to the character of future precipitation  
479 extremes.

480 Based on the above results, it is apparent that the magnitude of the effects of ENSO is compa-  
481 rable or even higher than the impacts of climate forcing – that is, shifts in the future character of  
482 ENSO would have more dire implications for precipitation extremes than shifts in mean climato-  
483 logical forcing. To investigate this further, linear regression has applied at each grid point using  
484 a simple linear model that incorporates the phase of ENSO (using the Niño 3.4 SST anomaly)  
485 and the underlying climate forcing (from mean GHG concentration). The precipitation indices are

486 used as response variables. The significance of these two factors was then obtained from ANOVA  
487 (analysis of variance) output (see the supplement [Paul: Point to lm\_fit\_pvalue]). The magnitude  
488 of the response associated with each factor was also computed (see the supplement [Paul: Point  
489 to wd\_lmfit\_coef\_enso\_ghg]). As expected, the ENSO forcing matches most closely with the dif-  
490 ference between El Niño and La Niña (see Figure 11). Hence, we observe that ENSO is a major  
491 driver of precipitation character through California, the intermountain west and the southwest and  
492 does have an impact on mean precipitation through the Cascades. In contrast, the impacts of cli-  
493 mate forcing are visually similar to the pattern of the difference between the different time periods  
494 (see Figure 6), and primarily impacts both extreme and non-extreme precipitation in the northwest  
495 and intermountain west.

496 We have also assessed the impacts of the Pacific Decadal Oscillation (PDO) on precipitation  
497 and observed only a weak correlation between the PDO pattern and precipitation. That is, pre-  
498 cipitation features did not change substantially between the cool phase or warm phase of PDO  
499 when examining hist data. However, when in phase with ENSO, PDO did have a notable impact  
500 over the northwest. This coupled effect has been found by studies such as Gershunov and Barnett  
501 (1998), who observed that ENSO and PDO can “reinforce” each other, with PDO responding to  
502 the same internal atmospheric variability as ENSO (Pierce 2002). In our simulations, there were  
503 roughly an equal number of positive PDO years and negative PDO years in the data from each  
504 time period, but since SSTs were fixed among ensemble members, the 26 year simulation period  
505 might be insufficient to account for the variability of PDO. Therefore, in this study we draw no  
506 conclusions on the impact of PDO.

507    **7. Discussion and Summary**

508    In this study, an ensemble of 26-year simulations have been conducted using VR-CESM with  
509    finest local grid resolution of  $\sim 0.25^\circ$  to assess the changing character of precipitation over the  
510    21st Century in the WUS. Climate forcing for future projections is prescribed under the RCP8.5  
511    “business-as-usual” scenario.

512    Evaluated against historical reanalysis and gridded data, VR-CESM was found to accurately cap-  
513    ture the spatial patterns of precipitation, including precipitation frequency and intensity, although it  
514    exhibited an overestimation of precipitation over the eastern flank of the Cascades, throughout Cal-  
515    ifornia’s Central Valley and along the Sierra Nevada. Nonetheless, there was clear improvement in  
516    the representation of precipitation features when compared with coarse  $1^\circ$  resolution simulations.

517    Both mean changes to precipitation and distributions of both non-extreme and extreme events  
518    projected by the VR-CESM model under climate forcing. Although constrained by water influx  
519    and soil moisture, changes to extreme precipitation are hypothesized to follow the C-C relationship  
520    more closely than total precipitation amount.

521    From the VR-CESM results, the warming response to the RCP8.5 climate forcing exhibited  
522    roughly uniform character, although warming was more pronounced away from the coast and to  
523    the north. Future relative humidity (RH) was observed to be constrained by competing increases  
524    in both temperature and atmospheric water vapor content. RH tended to increase in regions where  
525    average temperature increase was below  $\sim 2$  K, and decrease when average temperature increase  
526    exceeded  $\sim 2$  K. This suggests that continental evaporation and oceanic water vapor transport  
527    are insufficient vapor sources to maintain RH levels above a certain threshold temperature. In  
528    response, mean precipitation increase is fairly inhomogeneous, with a more pronounced increase  
529    in the Northwest where vapor transport is enhanced.

530 Over the intermountain west and southwest, an increase in warm season RH through mid-century  
531 led to a statistically significant increase in precipitation and non-extreme rainy days due to in-  
532 creased convection. This increase levels off through end-of-century, when increased temperatures  
533 are observed to drive a reduction in RH. Nonetheless, there is a significant increase in extreme  
534 precipitation episodes ( $\geq 10$  mm/day) over the intermountain west which is not observed in the  
535 southwest.

536 Over the northwest, there is a clear shift from non-extreme precipitation events to extreme pre-  
537 cipitation events associated with a moistening of the cool season and drying through the warm  
538 season. Although the total number of annual precipitation days remains relatively constant, there  
539 is a decrease in  $< 10$  mm/day precipitation days and an increase in  $> 20$  mm/day precipitation  
540 days. In each case, the change is on the order of 10 days/year. This change is driven by increased  
541 IVT over the eastern Pacific, associated with atmospheric river (AR) episodes. Increased drying  
542 over the warm season is driven by a reduction in RH. Increased cool season precipitation extremes  
543 in this region tend to result in high runoff events, which are in turn associated with a greater chance  
544 of flooding, particularly from rain-on-snow events.

545 Over California, except along the northernmost coast, there is no clear climate signal apparent  
546 in the mean precipitation or extremes. Interannual variability in this region associated with ENSO  
547 dominates precipitation patterns throughout the historical period and the 21st century. ENSO  
548 drives precipitation behavior by modulating the midlatitudinal storm track in this region. In par-  
549 ticular, during the El Niño phase, there is an increase in on-shore moisture flux over California  
550 that triggers a returning circulation through the northwest. The results over California highlight  
551 the importance of understanding the response of ENSO to climate change (which is still largely  
552 inconsistent in CMIP5 climate models and so is a key source of uncertainty in our results), since

553 variations in the magnitude or structure of ENSO will have immediate consequences for precipi-  
554 tation in this region.

555 The projected SSTs utilized for this study through end-of-century suggest that SST anomalies  
556 associated with ENSO will intensify. The impacts of ENSO are wide-reaching, with a statis-  
557 tically significant response observed in the character of precipitation throughout California, the  
558 intermountain west and the southwest regions, as well as impacting mean precipitation through  
559 the Cascades. In contrast, the significance of climate forcing (when compensating for ENSO)  
560 largely matched the differences observed between time periods, and had its greatest impact on  
561 both extreme and non-extreme precipitation in the northwest and intermountain west.

562 *Acknowledgments.* The authors would like to thank Michael Wehner for sharing the  $0.25^{\circ}$   
563 uniform-resolution CESM dataset, and his many suggestions. The authors also want to thank Alan  
564 M. Rhoades for providing the simulation output and providing his feedback on the manuscript.  
565 We acknowledge the substantial efforts behind the datasets used in this study, including UW,  
566 NCDC and NARR. The simulation data used is available by request at xyhuang@ucdavis.edu.  
567 This project is supported in part by the University of California, Davis and by the Department of  
568 Energy “Multiscale Methods for Accurate, Efficient, and Scale-Aware Models of the Earth Sys-  
569 tem” project. Support also comes from the California Agricultural Experiment Station (project  
570 CA-D-LAW-2203-H).

## 571 **References**

572 AchutaRao, K., and K. R. Sperber, 2006: Enso simulation in coupled ocean-atmosphere models:  
573 are the current models better? *Climate Dynamics*, **27** (1), 1–15.

- 574 Allan, R. P., and B. J. Soden, 2008: Atmospheric warming and the amplification of precipitation  
575 extremes. *Science*, **321** (5895), 1481–1484.
- 576 Allen, M. R., and W. J. Ingram, 2002: Constraints on future changes in climate and the hydrologic  
577 cycle. *Nature*, **419** (6903), 224–232.
- 578 Ashfaq, M., D. Rastogi, R. Mei, S.-C. Kao, S. Gangrade, B. Naz, and D. Touma, 2016: High-  
579 resolution ensemble projections of near-term regional climate over the continental united states.  
580 *Journal of Geophysical Research: Atmospheres*, doi:10.1002/2016JD025285.
- 581 Bell, J. L., L. C. Sloan, and M. A. Snyder, 2004: Regional changes in extreme climatic events: a  
582 future climate scenario. *Journal of Climate*, **17** (1), 81–87.
- 583 Cai, W., and Coauthors, 2014: Increasing frequency of extreme el niño events due to greenhouse  
584 warming. *Nature climate change*, **4** (2), 111–116.
- 585 Caldwell, P., 2010: California wintertime precipitation bias in regional and global climate models.  
586 *Journal of Applied Meteorology and Climatology*, **49** (10), 2147–2158.
- 587 Capotondi, A., 2013: Enso diversity in the ncar ccsm4 climate model. *Journal of Geophysical  
588 Research: Oceans*, **118** (10), 4755–4770.
- 589 Cayan, D. R., T. Das, D. W. Pierce, T. P. Barnett, M. Tyree, and A. Gershunov, 2010: Future  
590 dryness in the southwest us and the hydrology of the early 21st century drought. *Proceedings of  
591 the National Academy of Sciences*, **107** (50), 21 271–21 276.
- 592 Cayan, D. R., K. T. Redmond, and L. G. Riddle, 1999: ENSO and hydrologic extremes in the  
593 western United States\*. *Journal of Climate*, **12** (9), 2881–2893.
- 594 Collins, M., and Coauthors, 2010: The impact of global warming on the tropical pacific ocean and  
595 el niño. *Nature Geoscience*, **3** (6), 391–397.

- 596 Dennis, J., and Coauthors, 2011: CAM-SE: A scalable spectral element dynamical core for the  
597 Community Atmosphere Model. *International Journal of High Performance Computing Applications*,  
598 1094342011428142.
- 599 Deser, C., R. Knutti, S. Solomon, and A. S. Phillips, 2012a: Communication of the role of natural  
600 variability in future north american climate. *Nature Climate Change*, **2** (11), 775–779.
- 601 Deser, C., A. Phillips, V. Bourdette, and H. Teng, 2012b: Uncertainty in climate change projec-  
602 tions: the role of internal variability. *Climate Dynamics*, **38** (3-4), 527–546.
- 603 Deser, C., and Coauthors, 2012c: Enso and pacific decadal variability in the community climate  
604 system model version 4. *Journal of Climate*, **25** (8), 2622–2651.
- 605 Dettinger, M., 2011: Climate change, atmospheric rivers, and floods in california—a multimodel  
606 analysis of storm frequency and magnitude changes1. Wiley Online Library.
- 607 Diffenbaugh, N. S., J. S. Pal, R. J. Trapp, and F. Giorgi, 2005: Fine-scale processes regulate the  
608 response of extreme events to global climate change. *Proceedings of the National Academy of*  
609 *Sciences of the United States of America*, **102** (44), 15 774–15 778.
- 610 DiNezio, P. N., B. P. Kirtman, A. C. Clement, S.-K. Lee, G. A. Vecchi, and A. Wittenberg, 2012:  
611 Mean climate controls on the simulated response of enso to increasing greenhouse gases. *Jour-*  
612 *nal of Climate*, **25** (21), 7399–7420.
- 613 Dominguez, F., E. Rivera, D. Lettenmaier, and C. Castro, 2012: Changes in winter precipitation  
614 extremes for the western united states under a warmer climate as simulated by regional climate  
615 models. *Geophysical Research Letters*, **39** (5).
- 616 Donat, M. G., A. L. Lowry, L. V. Alexander, P. A. OGorman, and N. Maher, 2016: More extreme  
617 precipitation in the world’s dry and wet regions. *Nature Climate Change*.

- 618 Duffy, P., and Coauthors, 2006: Simulations of present and future climates in the western United  
619 States with four nested regional climate models. *Journal of Climate*, **19** (6), 873–895.
- 620 Duli re, V., Y. Zhang, and E. P. Salath  Jr, 2011: Extreme Precipitation and Temperature over the  
621 US Pacific Northwest: A Comparison between Observations, Reanalysis Data, and Regional  
622 Models\*. *Journal of Climate*, **24** (7), 1950–1964.
- 623 Easterling, D. R., G. A. Meehl, C. Parmesan, S. A. Changnon, T. R. Karl, and L. O. Mearns, 2000:  
624 Climate extremes: observations, modeling, and impacts. *science*, **289** (5487), 2068–2074.
- 625 Fedorov, A. V., and S. G. Philander, 2000: Is el ni o changing? *Science*, **288** (5473), 1997–2002.
- 626 Fox-Rabinovitz, M., J. C te, B. Dugas, M. D qu , and J. L. McGregor, 2006: Variable resolution  
627 general circulation models: Stretched-grid model intercomparison project (SGMIP). *Journal of  
628 Geophysical Research: Atmospheres (1984–2012)*, **111** (D16).
- 629 Fox-Rabinovitz, M. S., G. L. Stenchikov, M. J. Suarez, and L. L. Takacs, 1997: A finite-  
630 difference GCM dynamical core with a variable-resolution stretched grid. *Monthly weather  
631 review*, **125** (11), 2943–2968.
- 632 Frei, C., R. Sch ll, S. Fukutome, J. Schmidli, and P. L. Vidale, 2006: Future change of precipita-  
633 tion extremes in Europe: Intercomparison of scenarios from regional climate models. *Journal  
634 of Geophysical Research: Atmospheres (1984–2012)*, **111** (D6).
- 635 Gao, Y., J. Lu, L. R. Leung, Q. Yang, S. Hagos, and Y. Qian, 2015: Dynamical and thermodynamical  
636 modulations on future changes of landfalling atmospheric rivers over western north america.  
637 *Geophysical Research Letters*, **42** (17), 7179–7186.
- 638 Gates, W. L., 1992: AMIP: The Atmospheric Model Intercomparison Project. *Bulletin of the  
639 American Meteorological Society*, **73**, 1962–1970.

- 640 Gershunov, A., and T. P. Barnett, 1998: Interdecadal modulation of enso teleconnections. *Bulletin*  
641 *of the American Meteorological Society*, **79** (12), 2715–2725.
- 642 Gettelman, A., H. Morrison, and S. J. Ghan, 2008: A new two-moment bulk stratiform cloud  
643 microphysics scheme in the Community Atmosphere Model, version 3 (CAM3). Part II: Single-  
644 column and global results. *Journal of Climate*, **21** (15), 3660–3679.
- 645 Grodsky, S. A., J. A. Carton, S. Nigam, and Y. M. Okumura, 2012: Tropical atlantic biases in  
646 CCSM4. *Journal of Climate*, **25** (11), 3684–3701.
- 647 Guilyardi, E., A. Wittenberg, A. Fedorov, M. Collins, C. Wang, A. Capotondi, G. J. Van Olden-  
648 borgh, and T. Stockdale, 2009: Understanding el niño in ocean-atmosphere general circulation  
649 models. *Bulletin of the American Meteorological Society*, **90** (3), 325.
- 650 Hamlet, A. F., and D. P. Lettenmaier, 2005: Production of Temporally Consistent Gridded Precipi-  
651 tation and Temperature Fields for the Continental United States\*. *Journal of Hydrometeorology*,  
652 **6** (3), 330–336.
- 653 Hamlet, A. F., and D. P. Lettenmaier, 2007: Effects of 20th century warming and climate variability  
654 on flood risk in the western us. *Water Resources Research*, **43** (6).
- 655 Hegerl, G. C., F. W. Zwiers, P. A. Stott, and V. V. Kharin, 2004: Detectability of anthropogenic  
656 changes in annual temperature and precipitation extremes. *Journal of Climate*, **17** (19), 3683–  
657 3700.
- 658 Huang, X., A. M. Rhoades, P. A. Ullrich, and C. M. Zarzycki, 2016: An evaluation of the vari-  
659 able resolution-cesm for modeling california’s climate. *Journal of Advances in Modeling Earth*  
660 *Systems*.

- 661 Huang, X., and P. A. Ullrich, 2016: Irrigation impacts on California's climate with the variable-  
662 resolution CESM. *Journal of Advances in Modeling Earth Systems*.
- 663 Hurrell, J. W., J. J. Hack, D. Shea, J. M. Caron, and J. Rosinski, 2008: A new sea surface temper-  
664 ature and sea ice boundary dataset for the Community Atmosphere Model. *Journal of Climate*,  
665 **21** (19), 5145–5153.
- 666 Hurrell, J. W., and Coauthors, 2013: The community earth system model: A framework for col-  
667 laborative research. *Bulletin of the American Meteorological Society*, **94** (9), 1339–1360.
- 668 Jha, B., Z.-Z. Hu, and A. Kumar, 2014: Sst and enso variability and change simulated in historical  
669 experiments of cmip5 models. *Climate dynamics*, **42** (7-8), 2113–2124.
- 670 Joseph, R., and S. Nigam, 2006: Enso evolution and teleconnections in ipcc's twentieth-century  
671 climate simulations: Realistic representation? *Journal of Climate*, **19** (17), 4360–4377.
- 672 Joshi, M. M., J. M. Gregory, M. J. Webb, D. M. Sexton, and T. C. Johns, 2008: Mechanisms for  
673 the land/sea warming contrast exhibited by simulations of climate change. *Climate Dynamics*,  
674 **30** (5), 455–465.
- 675 Kahya, E., and J. A. Dracup, 1994: The influences of type 1 el nino and la nina events on stream-  
676 flows in the pacific southwest of the united states. *Journal of Climate*, **7** (6), 965–976.
- 677 Kao, H.-Y., and J.-Y. Yu, 2009: Contrasting eastern-pacific and central-pacific types of enso.  
678 *Journal of Climate*, **22** (3), 615–632.
- 679 Karl, T. R., N. Nicholls, and A. Ghazi, 1999: Clivar/gcos/wmo workshop on indices and indicators  
680 for climate extremes workshop summary. *Weather and Climate Extremes*, Springer, 3–7.

- 681 Kharin, V. V., F. W. Zwiers, X. Zhang, and G. C. Hegerl, 2007: Changes in temperature and  
682 precipitation extremes in the IPCC ensemble of global coupled model simulations. *Journal of*  
683 *Climate*, **20** (8), 1419–1444.
- 684 Kim, J., 2005: A projection of the effects of the climate change induced by increased co2 on  
685 extreme hydrologic events in the western us. *Climatic Change*, **68** (1-2), 153–168.
- 686 Laprise, R., and Coauthors, 2008: Challenging some tenets of regional climate modelling. *Meteo-*  
687 *rology and Atmospheric Physics*, **100** (1-4), 3–22.
- 688 Larkin, N. K., and D. Harrison, 2005: On the definition of el niño and associated seasonal average  
689 us weather anomalies. *Geophysical Research Letters*, **32** (13).
- 690 Latif, M., and N. S. Keenlyside, 2009: El niño/southern oscillation response to global warming.  
691 *Proceedings of the National Academy of Sciences*, **106** (49), 20 578–20 583.
- 692 Leung, L. R., L. O. Mearns, F. Giorgi, and R. L. Wilby, 2003a: Regional climate research: needs  
693 and opportunities. *Bulletin of the American Meteorological Society*, **84** (1), 89–95.
- 694 Leung, L. R., and Y. Qian, 2009: Atmospheric rivers induced heavy precipitation and flooding in  
695 the western US simulated by the WRF regional climate model. *Geophysical research letters*,  
696 **36** (3).
- 697 Leung, L. R., Y. Qian, and X. Bian, 2003b: Hydroclimate of the western United States based on  
698 observations and regional climate simulation of 1981-2000. Part I: Seasonal statistics. *Journal*  
699 *of Climate*, **16** (12), 1892–1911.
- 700 Maloney, E. D., and Coauthors, 2014: North american climate in cmip5 experiments: part iii:  
701 assessment of twenty-first-century projections\*. *Journal of Climate*, **27** (6), 2230–2270.

- 702 Maurer, E., A. Wood, J. Adam, D. Lettenmaier, and B. Nijssen, 2002: A long-term hydrologically  
703 based dataset of land surface fluxes and states for the conterminous United States\*. *Journal of*  
704 *climate*, **15 (22)**, 3237–3251.
- 705 McDonald, A., 2003: Transparent boundary conditions for the shallow-water equations: testing in  
706 a nested environment. *Monthly weather review*, **131 (4)**, 698–705.
- 707 Meehl, G. A., H. Teng, and G. Branstator, 2006: Future changes of el niño in two global coupled  
708 climate models. *Climate Dynamics*, **26 (6)**, 549–566.
- 709 Mesinger, F., and K. Veljovic, 2013: Limited area NWP and regional climate modeling: a test  
710 of the relaxation vs Eta lateral boundary conditions. *Meteorology and Atmospheric Physics*,  
711 **119 (1-2)**, 1–16.
- 712 Mesinger, F., and Coauthors, 2006: North American regional reanalysis. *Bulletin of the American*  
713 *Meteorological Society*, **87**, 343–360.
- 714 Min, S.-K., X. Zhang, F. W. Zwiers, and G. C. Hegerl, 2011: Human contribution to more-intense  
715 precipitation extremes. *Nature*, **470 (7334)**, 378–381.
- 716 Morrison, H., and A. Gettelman, 2008: A new two-moment bulk stratiform cloud microphysics  
717 scheme in the Community Atmosphere Model, version 3 (CAM3). Part I: Description and nu-  
718 matical tests. *Journal of Climate*, **21 (15)**, 3642–3659.
- 719 Neale, R. B., and Coauthors, 2010a: Description of the NCAR community atmosphere model  
720 (CAM 5.0). *NCAR Tech. Note NCAR/TN-486+STR*.
- 721 Neale, R. B., and Coauthors, 2010b: Description of the NCAR Community Atmosphere Model  
722 (CAM 5.0). NCAR Technical Note NCAR/TN-486+STR, National Center for Atmospheric Re-  
723 search, Boulder, Colorado, 268 pp.

- 724 Neelin, J. D., B. Langenbrunner, J. E. Meyerson, A. Hall, and N. Berg, 2013: California winter  
725 precipitation change under global warming in the coupled model intercomparison project phase  
726 5 ensemble. *Journal of Climate*, **26** (17), 6238–6256.
- 727 Neiman, P. J., F. M. Ralph, G. A. Wick, J. D. Lundquist, and M. D. Dettinger, 2008: Meteorolog-  
728 ical characteristics and overland precipitation impacts of atmospheric rivers affecting the west  
729 coast of north america based on eight years of ssm/i satellite observations. *Journal of Hydrom-  
730 eteorology*, **9** (1), 22–47.
- 731 NOAA, 2013: Defining El Niño and La Niña. Accessed: 2015-  
732 08-20, [https://www.climate.gov/news-features/understanding-climate/  
733 watching-el-nio-and-la-nia-noaa-adapts-global-warming](https://www.climate.gov/news-features/understanding-climate/watching-el-nio-and-la-nia-noaa-adapts-global-warming).
- 734 O’Gorman, P. A., and T. Schneider, 2009: The physical basis for increases in precipitation ex-  
735 tremes in simulations of 21st-century climate change. *Proceedings of the National Academy of  
736 Sciences*, **106** (35), 14 773–14 777.
- 737 Oleson, K., and Coauthors, 2010: Technical description of version 4.0 of the Community Land  
738 Model (CLM). NCAR Technical Note NCAR/TN-478+STR, National Center for Atmospheric  
739 Research, Boulder, Colorado, 257 pp. doi:10.5065/D6FB50WZ.
- 740 Pierce, D. W., 2002: The role of sea surface temperatures in interactions between enso and the  
741 north pacific oscillation. *Journal of climate*, **15** (11), 1295–1308.
- 742 Ralph, F. M., P. J. Neiman, and G. A. Wick, 2004: Satellite and caljet aircraft observations of  
743 atmospheric rivers over the eastern north pacific ocean during the winter of 1997/98. *Monthly  
744 Weather Review*, **132** (7), 1721–1745.

- 745 Rauscher, S. A., E. Coppola, C. Piani, and F. Giorgi, 2010: Resolution effects on regional climate  
746 model simulations of seasonal precipitation over Europe. *Climate dynamics*, **35** (4), 685–711.
- 747 Rauscher, S. A., T. D. Ringler, W. C. Skamarock, and A. A. Mirin, 2013: Exploring a Global  
748 Multiresolution Modeling Approach Using Aquaplanet Simulations. *Journal of Climate*, **26** (8),  
749 2432–2452.
- 750 Rhoades, A. M., X. Huang, P. A. Ullrich, and C. M. Zarzycki, 2015: Characterizing Sierra Nevada  
751 snowpack using variable-resolution CESM. *Journal of Applied Meteorology and Climatology*,  
752 (2015).
- 753 Rhoades, P. U., A.M., and C. Zarzycki, 2016: Projecting 21st century snowpack trends in western  
754 usa mountains using variable-resolution cesm. *Climate Dynamics*.
- 755 Riahi, K., and Coauthors, 2011: RCP 8.5A scenario of comparatively high greenhouse gas emis-  
756 sions. *Climatic Change*, **109** (1-2), 33–57.
- 757 Rowell, D. P., and R. G. Jones, 2006: Causes and uncertainty of future summer drying over europe.  
758 *Climate Dynamics*, **27** (2-3), 281–299.
- 759 Salathé Jr, E. P., R. Steed, C. F. Mass, and P. H. Zahn, 2008: A High-Resolution Climate Model  
760 for the US Pacific Northwest: Mesoscale Feedbacks and Local Responses to Climate Change\*.  
761 *Journal of Climate*, **21** (21), 5708–5726.
- 762 Scoccimarro, E., M. Zampieri, A. Bellucci, A. Navarra, and Coauthors, 2013: Heavy precipitation  
763 events in a warmer climate: results from CMIP5 models. *Journal of climate*.
- 764 Seneviratne, S. I., and Coauthors, 2012: Changes in climate extremes and their impacts on the  
765 natural physical environment. *Managing the risks of extreme events and disasters to advance*  
766 *climate change adaptation*, 109–230.

- 767 Sillmann, J., V. Kharin, F. Zwiers, X. Zhang, and D. Bronaugh, 2013: Climate extremes indices  
768 in the cmip5 multimodel ensemble: Part 2. future climate projections. *Journal of Geophysical*  
769 *Research: Atmospheres*, **118 (6)**, 2473–2493.
- 770 Simmons, A., K. Willett, P. Jones, P. Thorne, and D. Dee, 2010: Low-frequency variations  
771 in surface atmospheric humidity, temperature, and precipitation: Inferences from reanalyses  
772 and monthly gridded observational data sets. *Journal of Geophysical Research: Atmospheres*,  
773 **115 (D1)**.
- 774 Singh, D., M. Tsiang, B. Rajaratnam, and N. S. Diffenbaugh, 2013: Precipitation extremes over the  
775 continental United States in a transient, high-resolution, ensemble climate model experiment.  
776 *Journal of Geophysical Research: Atmospheres*, **118 (13)**, 7063–7086.
- 777 Small, R. J., and Coauthors, 2014: A new synoptic scale resolving global climate simulation using  
778 the community earth system model. *Journal of Advances in Modeling Earth Systems*, **6 (4)**,  
779 1065–1094.
- 780 Staniforth, A. N., and H. L. Mitchell, 1978: A variable-resolution finite-element technique for  
781 regional forecasting with the primitive equations. *Monthly Weather Review*, **106 (4)**, 439–447.
- 782 Stephens, G. L., and Coauthors, 2010: Dreary state of precipitation in global models. *Journal of*  
783 *Geophysical Research: Atmospheres*, **115 (D24)**.
- 784 Stevenson, S., 2012: Significant changes to enso strength and impacts in the twenty-first century:  
785 Results from cmip5. *Geophysical Research Letters*, **39 (17)**.
- 786 Sugi, M., and J. Yoshimura, 2004: A mechanism of tropical precipitation change due to co2  
787 increase. *Journal of climate*, **17 (1)**, 238–243.

- 788 Taschetto, A. S., A. S. Gupta, N. C. Jourdain, A. Santoso, C. C. Ummenhofer, and M. H. England,  
789 2014: Cold tongue and warm pool enso events in cmip5: mean state and future projections.  
790 *Journal of Climate*, **27 (8)**, 2861–2885.
- 791 Taylor, M. A., 2011: Conservation of mass and energy for the moist atmospheric primitive equa-  
792 tions on unstructured grids. *Numerical Techniques for Global Atmospheric Models*, Springer,  
793 357–380.
- 794 Tebaldi, C., K. Hayhoe, J. M. Arblaster, and G. A. Meehl, 2006: Going to the extremes. *Climatic  
795 change*, **79 (3-4)**, 185–211.
- 796 Trenberth, K. E., 2011: Changes in precipitation with climate change. *Climate Research*, **47 (1)**,  
797 123.
- 798 Trenberth, K. E., A. Dai, R. M. Rasmussen, and D. B. Parsons, 2003: The changing character of  
799 precipitation. *Bulletin of the American Meteorological Society*, **84 (9)**, 1205–1217.
- 800 Ullrich, P. A., D. Devendran, and H. Johansen, 2016: Arbitrary-order conservative and consistent  
801 remapping and a theory of linear maps, part 2. *Monthly Weather Review*, **144 (4)**, 1529–1549,  
802 doi:10.1175/MWR-D-15-0301.1.
- 803 Ullrich, P. A., and M. A. Taylor, 2015: Arbitrary-Order Conservative and Consistent Remapping  
804 and a Theory of Linear Maps: Part I. *Monthly Weather Review*, **143 (6)**, 2419–2440, doi:10.  
805 1175/MWR-D-14-00343.1.
- 806 Walker, M. D., and N. S. Diffenbaugh, 2009: Evaluation of high-resolution simulations of daily-  
807 scale temperature and precipitation over the united states. *Climate dynamics*, **33 (7-8)**, 1131–  
808 1147.

- 809 Wehner, M. F., 2013: Very extreme seasonal precipitation in the NARCCAP ensemble: model  
810 performance and projections. *Climate Dynamics*, **40** (1-2), 59–80.
- 811 Wehner, M. F., R. L. Smith, G. Bala, and P. Duffy, 2010: The effect of horizontal resolution  
812 on simulation of very extreme US precipitation events in a global atmosphere model. *Climate*  
813 *dynamics*, **34** (2-3), 241–247.
- 814 Wehner, M. F., and Coauthors, 2014: The effect of horizontal resolution on simulation qual-  
815 ity in the Community Atmospheric Model, CAM5.1. *J. Model. Earth. Sys.*, doi:10.1002/  
816 2013MS000276.
- 817 Yoon, J.-H., S. S. Wang, R. R. Gillies, B. Kravitz, L. Hipps, and P. J. Rasch, 2015: Increasing  
818 water cycle extremes in California and in relation to ENSO cycle under global warming. *Nature*  
819 *communications*, **6**.
- 820 Zarzycki, C. M., C. Jablonowski, and M. A. Taylor, 2014: Using Variable-Resolution Meshes  
821 to Model Tropical Cyclones in the Community Atmosphere Model. *Monthly Weather Review*,  
822 **142** (3), 1221–1239.
- 823 Zarzycki, C. M., C. Jablonowski, D. R. Thatcher, and M. A. Taylor, 2015: Effects of localized grid  
824 refinement on the general circulation and climatology in the Community Atmosphere Model.  
825 *Journal of Climate*, (2015).
- 826 Zhang, X., L. Alexander, G. C. Hegerl, P. Jones, A. K. Tank, T. C. Peterson, B. Trewin, and  
827 F. W. Zwiers, 2011: Indices for monitoring changes in extremes based on daily temperature and  
828 precipitation data. *Wiley Interdisciplinary Reviews: Climate Change*, **2** (6), 851–870.

<sup>829</sup> Zhang, X., J. Wang, F. W. Zwiers, and P. Y. Groisman, 2010: The influence of large-scale climate  
<sup>830</sup> variability on winter maximum daily precipitation over North America. *Journal of Climate*,  
<sup>831</sup> **23** (**11**), 2902–2915.

832 **LIST OF TABLES**

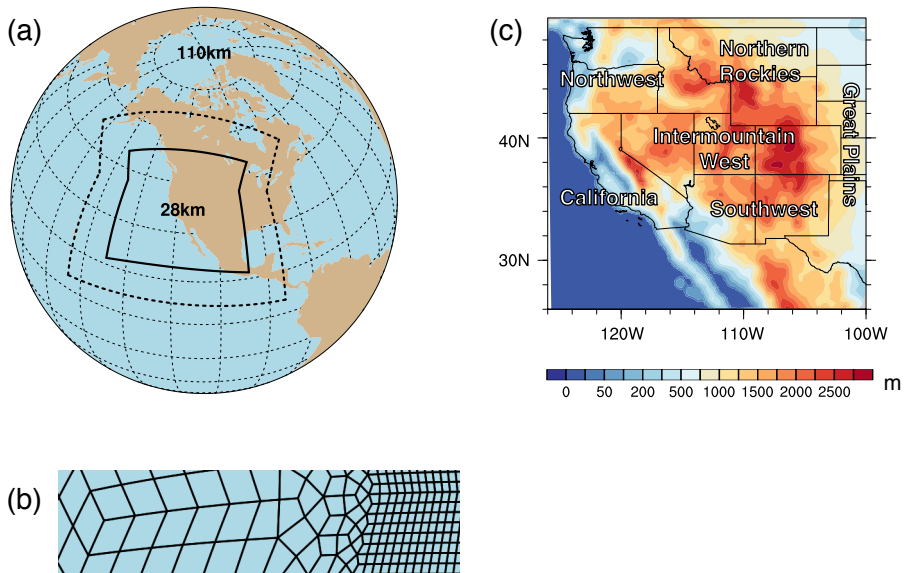
833 **Table 1.** Precipitation indices employed in this study. . . . . . . . . . . . . . . . 41

TABLE 1. Precipitation indices employed in this study.

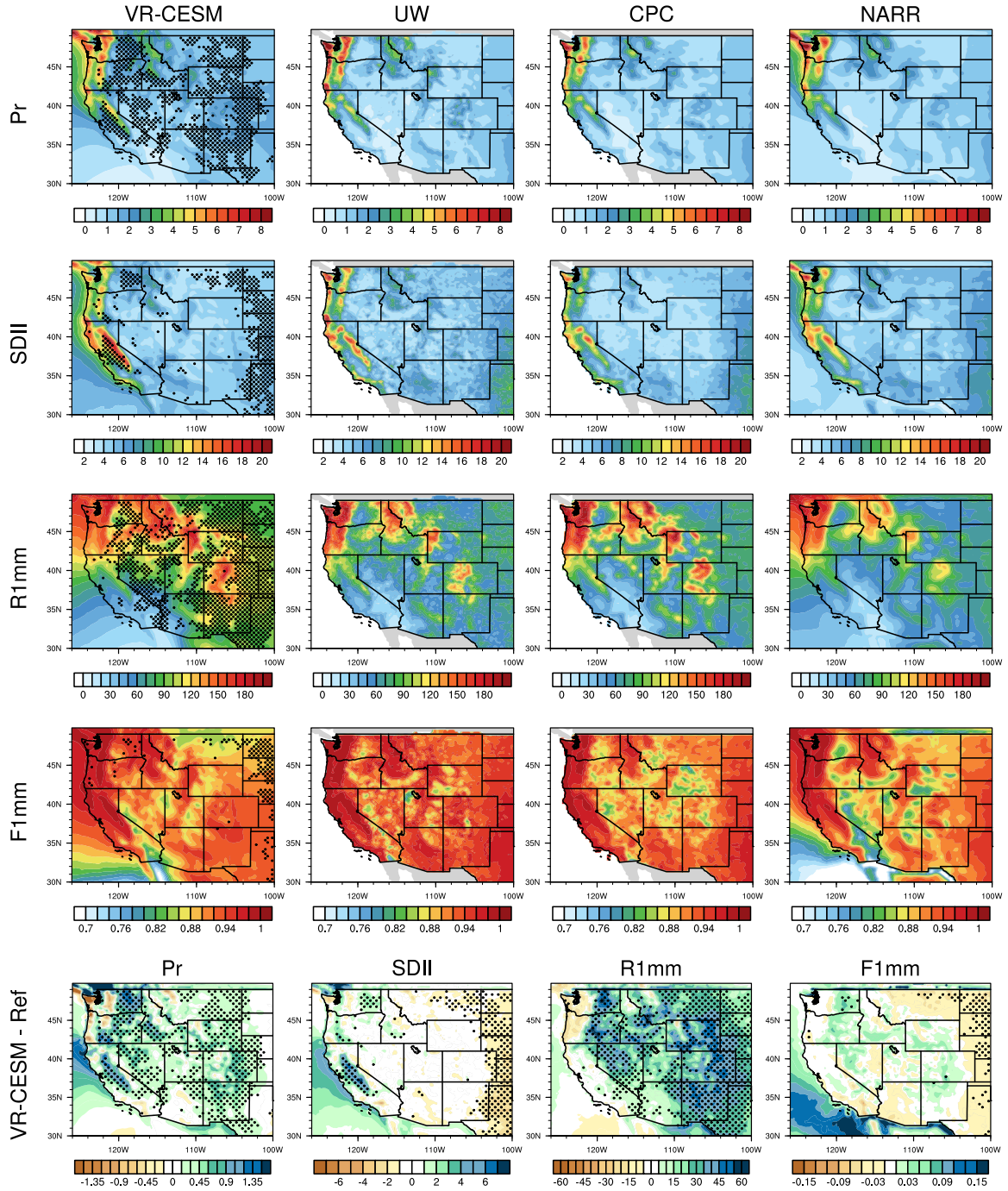
Indice	Definition
Pr	Mean daily precipitation
R1mm	Number of days per year with Pr>1 mm
SDII	Simple precipitation intensity index: Precipitation amount / $\langle R1mm \rangle$ (mm/day)
R5mm	Number of days per year with Pr>1 mm and Pr=<5 mm
R10mm	Number of days per year with Pr>5 mm and Pr=<10 mm
R20mm	Number of days per year with Pr>10 mm and Pr=<20 mm
R40mm	Number of days per year with Pr>20 mm and Pr=<40 mm
Rxmm	Number of days per year with Pr>40 mm
F1mm	Fraction of precipitation contributed to the total precipitation for days of R1mm (similarly for F5mm, F10mm, F20mm, F40mm and Fxmm)
P5mm	Precipitation amount from R5mm (similarly for P10mm, P20mm, F40mm, Pxmm)

## 834 LIST OF FIGURES

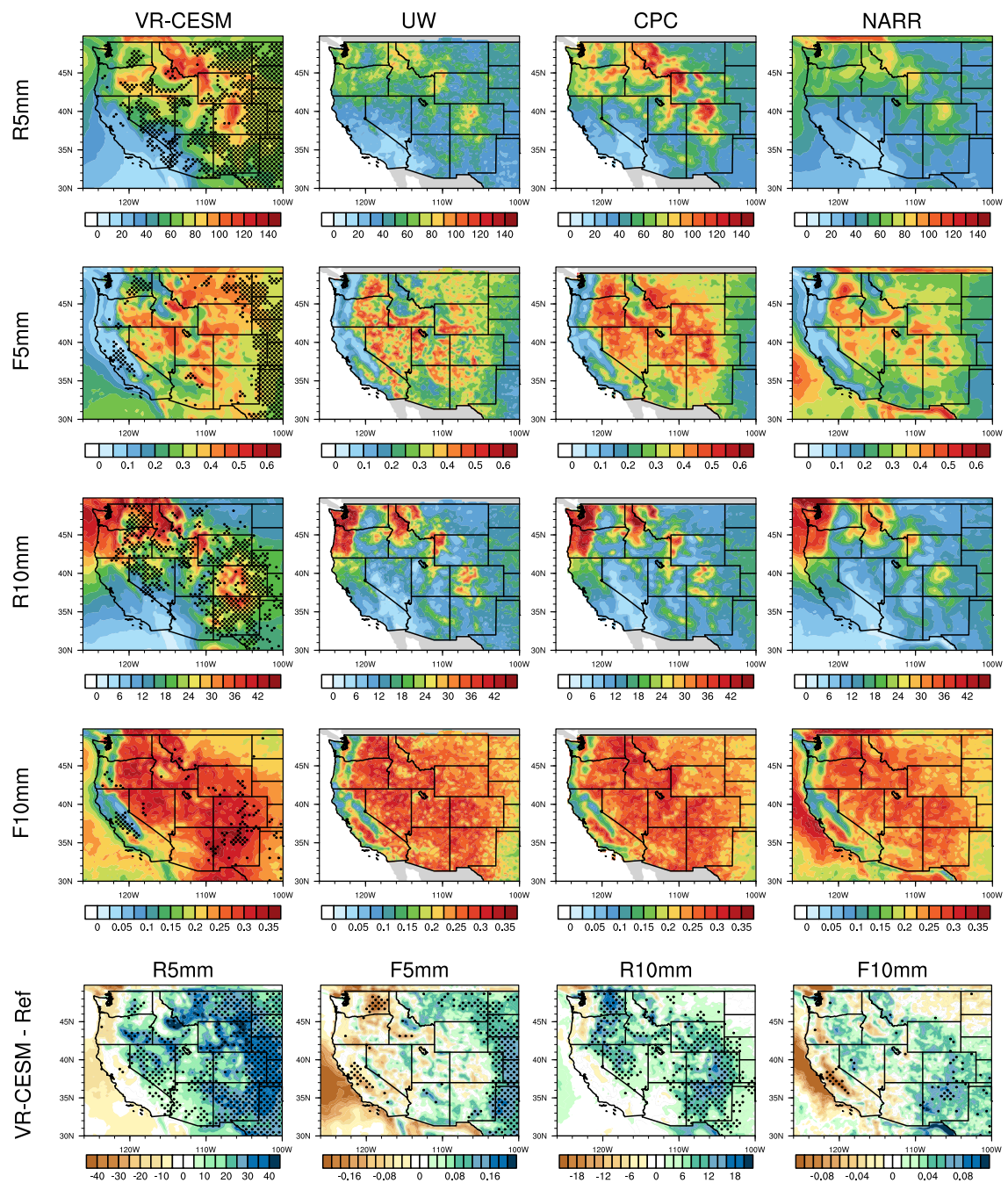
835	<b>Fig. 1.</b> (a) The approximate grid spacing used for the VR-CESM $0.25^\circ$ mesh. (b) A depiction of 836 the transition from the global $1^\circ$ resolution mesh through two layers of refinement to $0.25^\circ$ . 837 (c) Topography height over the study area. . . . .	43
838	<b>Fig. 2.</b> Mean precipitation and associated indices from VR-CESM and reference datasets over the 839 historical period, 1980-2005. Areas with statistically significance differences are marked 840 with stippling. . . . .	44
841	<b>Fig. 3.</b> Mean precipitation and associated indices from VR-CESM and reference datasets over the 842 historical period, 1980-2005 (continued). . . . .	45
843	<b>Fig. 4.</b> Mean precipitation and associated indices from VR-CESM and reference datasets over the 844 historical period, 1980-2005 (continued). . . . .	46
845	<b>Fig. 5.</b> The mean precipitation ( $Pr$ ), 2m average temperature ( $Tavg$ ), and 2m relative humidity ( $RH$ ) 846 averaged over each time period. Areas with statistically significance differences are marked 847 with stippling. . . . .	47
848	<b>Fig. 6.</b> Differences of precipitation indices $Pr$ (mm/day), SDII and $R*mm$ between hist, mid and 849 end average. Areas with statistically significance differences are marked with stippling. . . . .	48
850	<b>Fig. 7.</b> Differences of precipitation indices $Pr$ (mm/year) and $P*mm$ between hist, mid and end 851 average. Areas with statistically significance differences are marked with stippling. . . . .	49
852	<b>Fig. 8.</b> Changes of specific humidity and horizontal wind pattern at 850hPa for moisture flux il- 853 lustration, and IVT for simulations under different time period of wet season (October to 854 March) averaged over 26 years. (Note: The minimum wind vector is set to be 0.5 m/s, 855 therefore, the wind less than 0.5 m/s is also plotted at the minimum length for better vis- 856 ulation.) <b>Specific humidity and wind pattern are averaged over all days over cool season</b> 857 <b>rather than days with <math>Pr \geq 10\text{mm}</math>.</b> . . . . .	50
858	<b>Fig. 9.</b> Frequency distribution of rainy days ( $Pr \geq 0.1\text{mm/day}$ ) over the three time periods from 859 simulations in four regions (with logarithmic vertical scale). (Note: Region (a) to (d) cover 860 Washington and Oregon; California (except northern part, i.e. latitude no larger than $38^\circ$ ); 861 Nevada and Utah; Arizona and New Mexico, respectively.) . . . . .	51
862	<b>Fig. 10.</b> Differences of precipitation indices $Pr$ and $R*mm$ between warm and cool phases of ENSO 863 over each time period. . . . .	52
864	<b>Fig. 11.</b> Changes of IVT for simulations under different phases of ENSO of wet season (October to 865 March) over rainy days averaged yearly, with seasonal mean wind patterns at 850hPa (Note: 866 The minimum wind vector is set to be 0.5 m/s, therefore, the wind less than 0.5 m/s is also 867 plotted at the minimum length for better visualization.) . . . . .	53



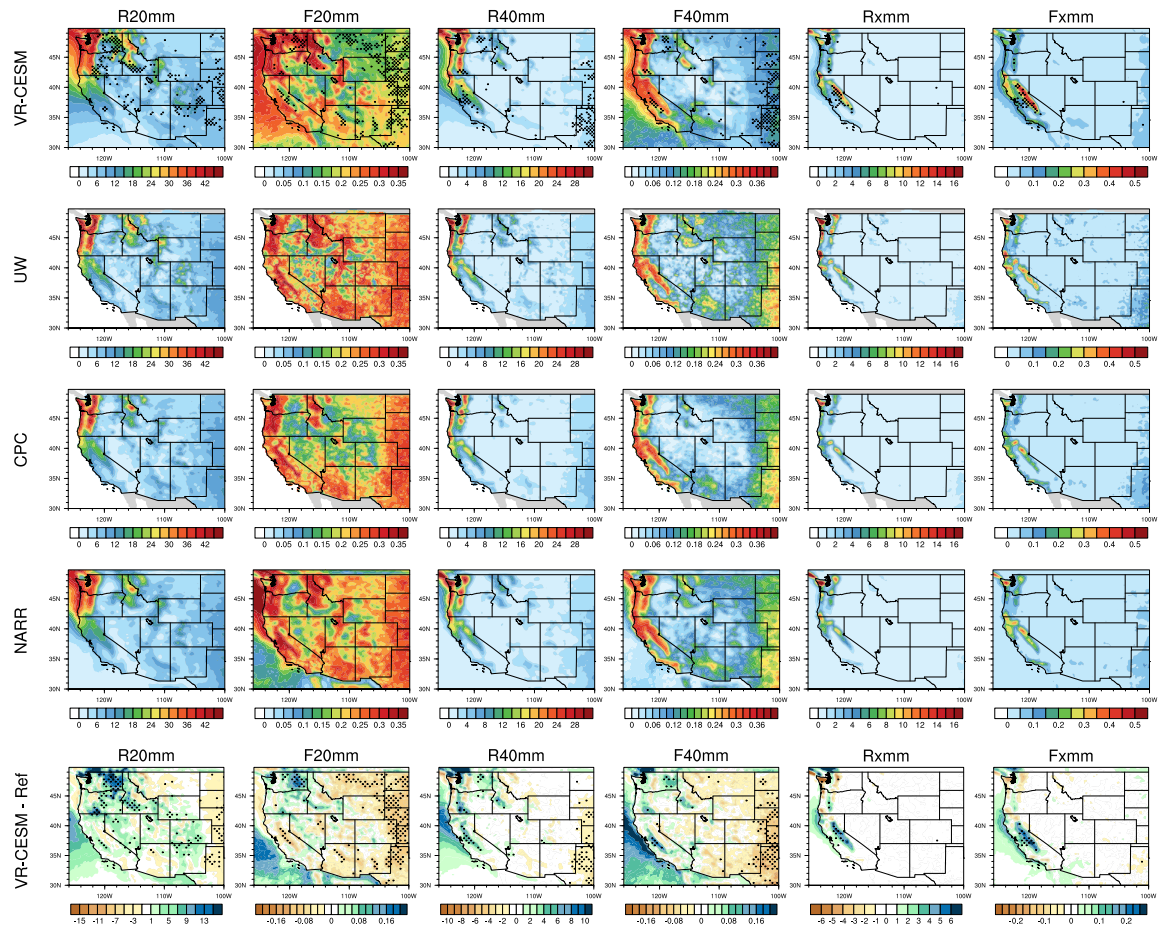
868 FIG. 1. (a) The approximate grid spacing used for the VR-CESM  $0.25^\circ$  mesh. (b) A depiction of the transition  
 869 from the global  $1^\circ$  resolution mesh through two layers of refinement to  $0.25^\circ$ . (c) Topography height over the  
 870 study area.



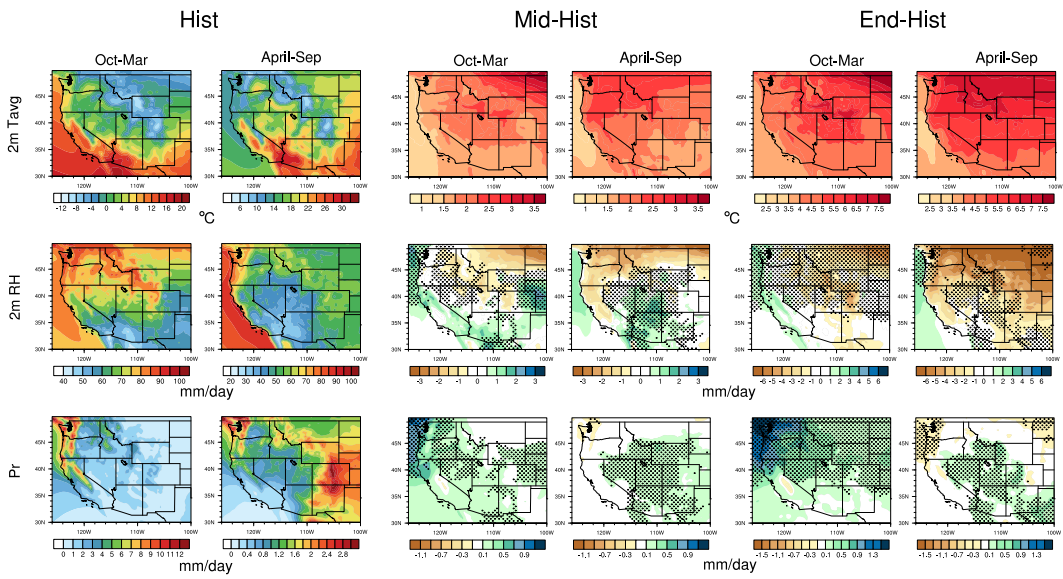
871 FIG. 2. Mean precipitation and associated indices from VR-CESM and reference datasets over the historical  
872 period, 1980-2005. Areas with statistically significant differences are marked with stippling.



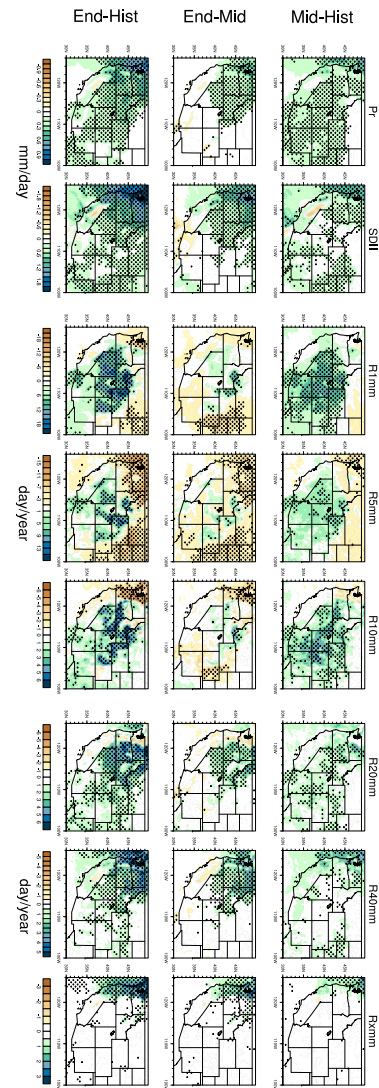
873 FIG. 3. Mean precipitation and associated indices from VR-CESM and reference datasets over the historical  
 874 period, 1980-2005 (continued).



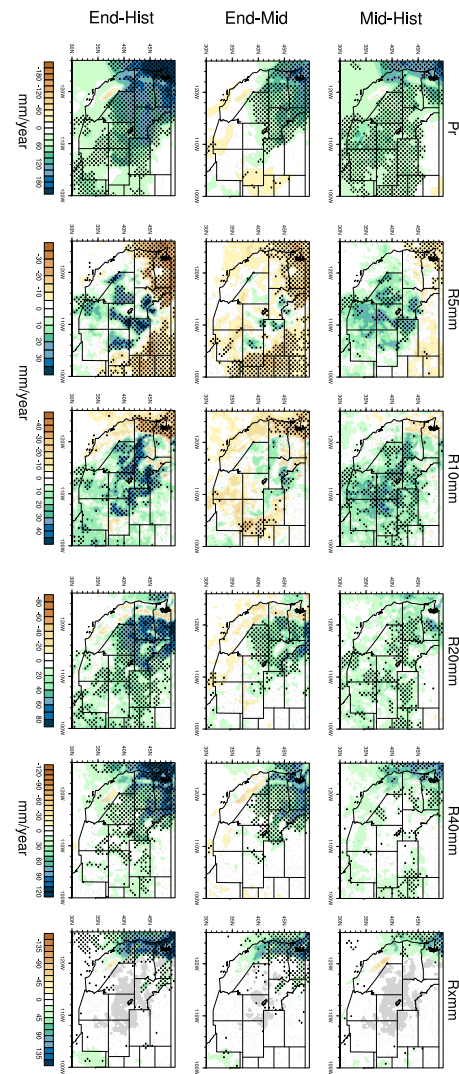
875 FIG. 4. Mean precipitation and associated indices from VR-CESM and reference datasets over the historical  
 876 period, 1980-2005 (continued).



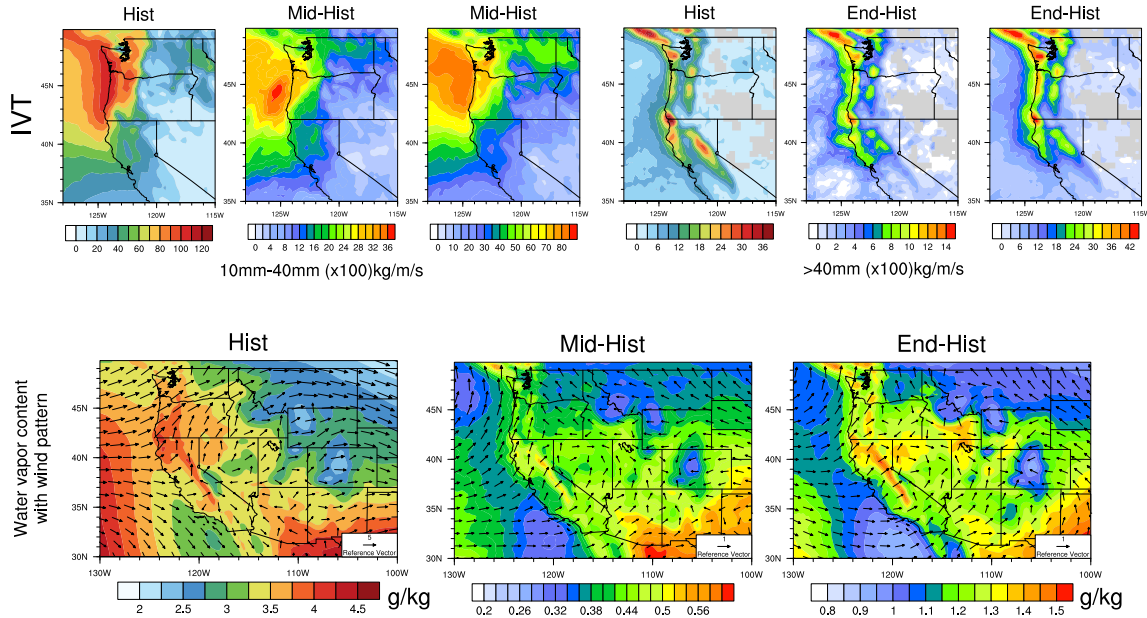
877 FIG. 5. The mean precipitation (Pr), 2m average temperature (Tavg), and 2m relative humidity (RH) averaged  
878 over each time period. Areas with statistically significance differences are marked with stippling.



879 FIG. 6. Differences of precipitation indices  $Pr$  (mm/day), SDII and  $R*mm$  between hist, mid and end average.  
 880 Areas with statistically significance differences are marked with stippling.



881 FIG. 7. Differences of precipitation indices  $Pr$  (mm/year) and  $P \cdot mm$  between hist, mid and end average.  
 882 Areas with statistically significance differences are marked with stippling.



883 FIG. 8. Changes of specific humidity and horizontal wind pattern at 850hPa for moisture flux illustration,  
 884 and IVT for simulations under different time period of wet season (October to March) averaged over 26 years.  
 885 (Note: The minimum wind vector is set to be 0.5 m/s, therefore, the wind less than 0.5 m/s is also plotted at the  
 886 minimum length for better visualization.) **Specific humidity and wind pattern are averaged over all days over**  
 887 **cool season rather than days with  $\text{Pr}_t > 10\text{mm}$ .**

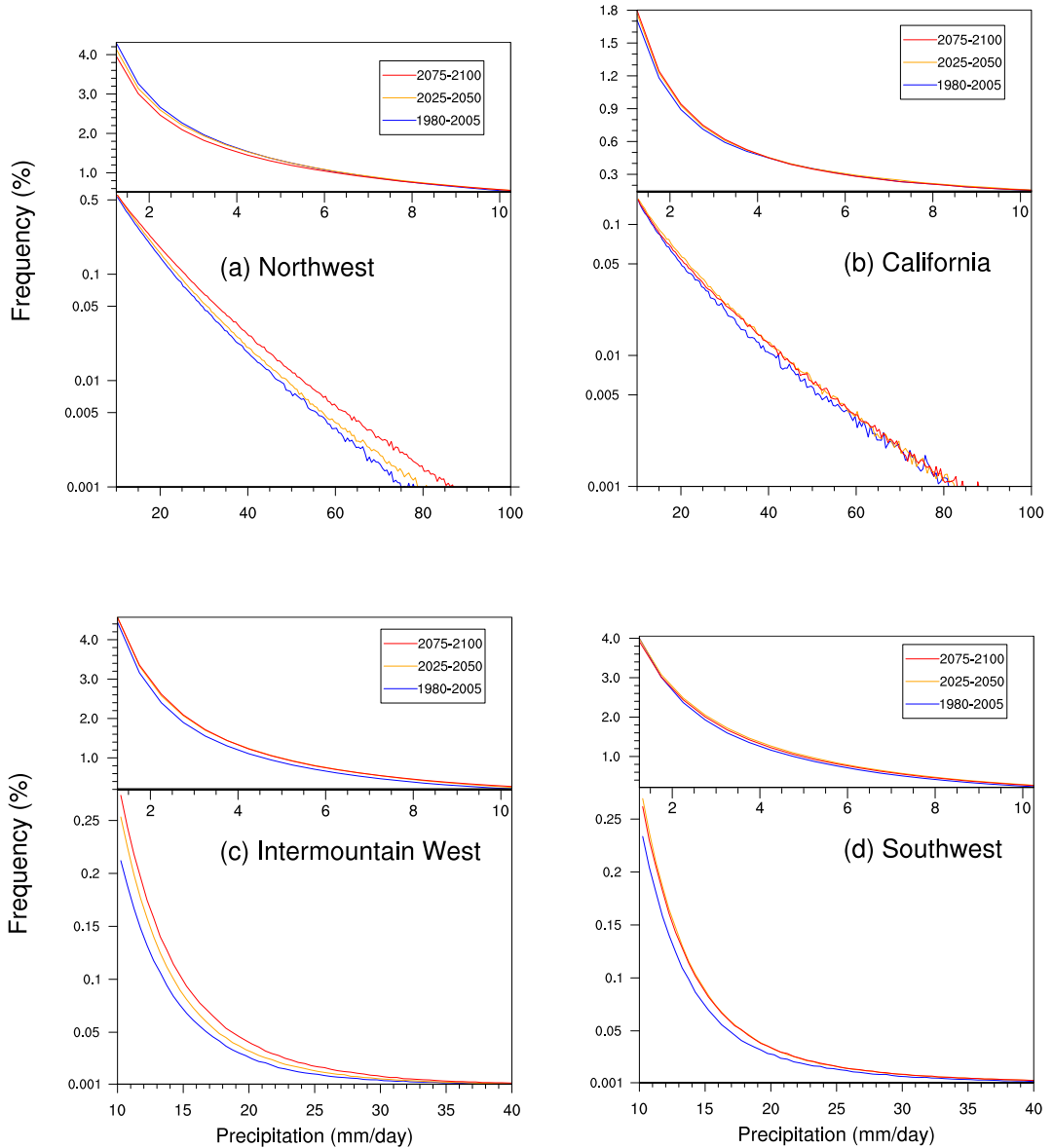
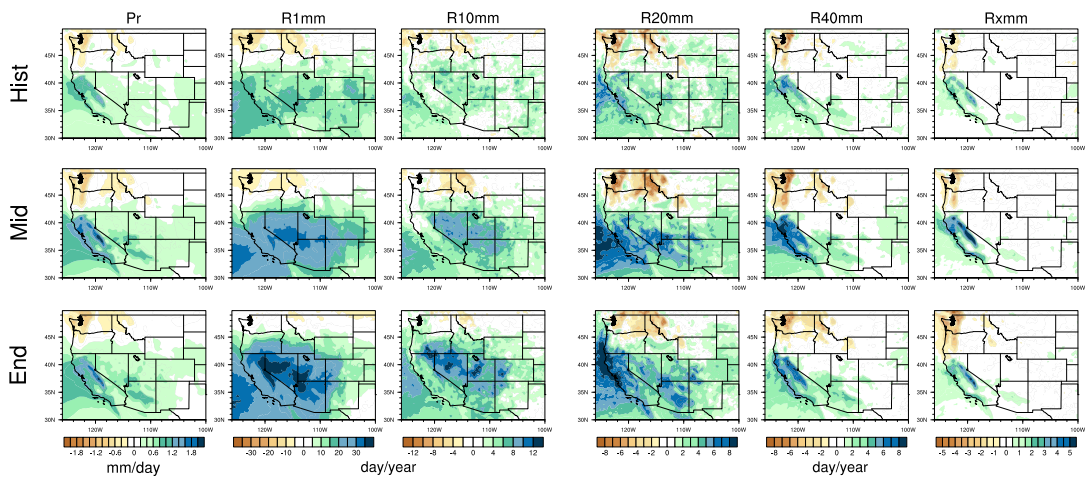
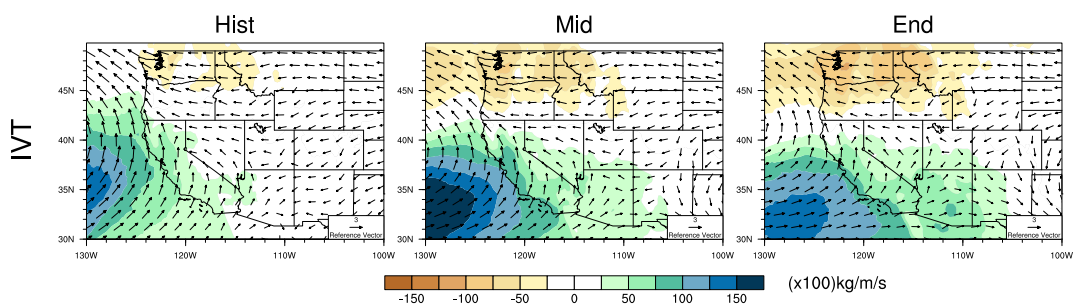


FIG. 9. Frequency distribution of rainy days ( $\text{Pr} \geq 0.1 \text{ mm/day}$ ) over the three time periods from simulations in four regions (with logarithmic vertical scale). (Note: Region (a) to (d) cover Washington and Oregon; California (except northern part, i.e. latitude no larger than  $38^\circ$ ); Nevada and Utah; Arizona and New Mexico, respectively.)



892 FIG. 10. Differences of precipitation indices Pr and R\*mm between warm and cool phases of ENSO over  
 893 each time period.



894 FIG. 11. Changes of IVT for simulations under different phases of ENSO of wet season (October to March)  
 895 over rainy days averaged yearly, with seasonal mean wind patterns at 850hPa (Note: The minimum wind vector  
 896 is set to be 0.5 m/s, therefore, the wind less than 0.5 m/s is also plotted at the minimum length for better  
 897 visualization.)